ARTICLE

Alan G. Galley

Composite synvolcanic intrusions associated with Precambrian VMS-related hydrothermal systems

Abstract Large subvolcanic intrusions are recognized within most Precambrian VMS camps. Of these, 80% are quartz diorite–tonalite–trondhjemite composite intrusions. The VMS camps spatially associated with composite intrusions account for >90% of the aggregate sulfide tonnage of all the Precambrian, intrusion-related VMS camps. These low-alumina, low-K, and high-Na composite intrusions contain early phases of quartz diorite and tonalite, followed by more voluminous trondhjemite. They have a high proportion of high silica (>74% SiO_2) trondhjemite which is compositionally similar to the VMS-hosting rhyolites within the volcanic host-rock successions. The quartz-diorite and possibly tonalite phases follow tholeiitic fractionation trends whereas the trondhjemites fall within the composition field for primitive crustal melts. These transitional M-I-type primitive intrusive suites are associated with extensional regimes within oceanic-arc environments. Subvolcanic composite intrusions related to the Archean Sturgeon Lake and Noranda, and Paleoproterozoic Snow Lake VMS camps range in volume from 300 to 1,000 km^3. Three have a sill morphology with strike lengths between 15 and 22 km and an average thickness between 1,500 and 2,000 m. The fourth has a gross stock-like shape. The VMS deposits are principally restricted to the volcanic strata above the strike length of the intrusions, as are areally extensive, thin exhalite units. The composite intrusions contain numerous internal phases which are commonly clustered within certain parts of the composite intrusion. These clusters underlie eruptive centers surrounded by areas of hydrothermal alteration and which contain most of the VMS deposits. Early quartz-diorite and tonalite phases appear to have intruded in rapid succession. Evidence includes gradational contacts, magma mixing and disequilibrium textures. They appear to have been emplaced as sill-dike swarms. These early phases are present as pendants and xenoliths within later trondhjemite phases. The trondhjemite phases contain numerous internal contacts indicating emplacement as composite sills. Common structural features of the composite intrusions include early xenolith phases, abundant small comagmatic dikes, fractures and veins and, in places, columnar jointing. Internal phases may differ greatly in texture from fine- to coarse-grained, aphyric and granophyric through seriate to porphyritic. Mineralogical and isotopic evidence indicates that early phases of each composite intrusion are affected by pervasive to fracture-controlled high-temperature (350–450 °C) alteration reflecting seawater-rock interaction. Trondhjemite phases contain hydrothermal-magmatic alteration assemblages within miarolitic cavities, hydrothermal breccias and veins. This hydrothermal-magmatic alteration may, in part, be inherited from previously altered wall rocks. Two of the four intrusions are host to Cu-Mo-rich intrusive breccias and porphyry-type mineralization which formed as much as 14 Ma after the main subvolcanic magmatic activity. The recognition of these Precambrian, subvolcanic composite intrusions is important for greenfields VMS exploration, as they define the location of thermal corridors within extensional oceanic-arc regimes which have the greatest potential for significant VMS mineralization. The VMS mineralization may occur for 2,000 m above the intrusions. In some cases, VMS mineralization has been truncated or enveloped by late trondhjemite phases of the composite intrusions. Evidence that much of the trondhjemitic magmatism postdates the principal VMS activity is a critical factor when developing heat and fluid flow models for these subseafloor magmatic-hydrothermal systems.

Keywords VMS deposits · Subvolcanic · Low-alumina tonalite–trondhjemite · Extensional environments · Large-scale alteration systems

A.G. Galley
Geological Survey of Canada, 601 Booth St.,
K1A 0E8 Ottawa ON, Canada
E-mail: agalley@NRCan.gc.ca
Tel.: +1-613-992-7867
Fax: +1-613-996-9820

Introduction

Synvolcanic intrusions have long been cited as the heat engines which initiate and sustain subseafloor hydrothermal systems which, in turn, form volcanogenic massive sulfide (VMS) deposits on, or near, the seafloor (Spooner and Fyfe 1973; Goldie 1976; Cathles 1977; Franklin et al. 1981; Campbell et al. 1981; Galley 1993, 1996). There is also speculation that these intrusions supply metals to the convecting hydrothermal system (Yang and Scott 1996; Sillitoe et al. 1996; Hannington et al. 1999). Modeling the role of large subseafloor intrusions in relation to VMS hydrothermal systems is based on observations from many massive sulfide districts around the world which range in age from Archean to Cretaceous (Table 1), as well as through deep-sea drilling and geophysical studies on the modern seafloor (Collier and Sinha 1990; Detrick 1991; Stinton and Detrick 1992; Calvert 1995; Alt 1995; Singh et al. 1999). Empirical evidence for this link includes not only the spatial association of subvolcanic intrusions with clusters of VMS deposits, but also the association between intrusion and broad-scale, semiconformable synvolcanic alteration zones (Spooner and Fyfe 1973; Gibson and Watkinson 1990; Stakes and Taylor 1992; Cathles 1993; Galley 1993; Taylor and Holk 1998; Bailes and Galley 1999; Hannington et al. 2002, this volume).

A number of large synvolcanic intrusions in close spatial association with VMS deposits are recorded in Table 1. The majority of these are Archean or Paleoproterozoic in age. Of the Precambrian synvolcanic intrusions associated with VMS mineralization, more than 80% are dominated by tonalite–trondhjemite phases. The VMS camps spatially associated with quartz diorite–tonalite–trondhjemite (henceforth referred to as composite) intrusions account for more than 90% of the aggregate sulfide tonnage of all the Precambrian, intrusion-related VMS camps.

In order to investigate the significance of these statistics, a four-year study was instigated by the Canadian Mining Industry Research Organization (CAMIRO Project 94E07) to investigate the relationships between synvolcanic composite intrusions, regional-scale alteration zones and VMS deposits. Study sites included the Archean Noranda (Quebec) and Sturgeon Lake (Ontario) VMS camps, and the Paleoproterozoic Snow Lake (Manitoba; Fig. 1) and Kristineberg (Sweden) VMS camps. The results from the three Canadian camps will be presented in this paper.

The objectives of this paper are to (1) define the physical and geochemical nature of the Beidelman Bay (BBIC), Flavrian-Powell (FPIC), Sneath Lake (SLIC) and Richard Lake (RLIC) subvolcanic intrusive complexes associated with the Sturgeon Lake, Noranda and Snow Lake VMS camps (Fig. 2A–C), and (2) to describe the role of tonalite–trondhjemite intrusions in generating VMS-related, subseafloor hydrothermal systems.

All four composite intrusions have a strong spatial relationship with clusters of VMS deposits, in that they are located within 2,000 m of the stratigraphic foot wall to VMS-hosting strata (Fig. 2A–C). All significant VMS mineralization and associated hydrothermal alteration in the volcanic host-rock succession is restricted to the strata which overlie each of the intrusions. The composite intrusions are geochemically similar to the overlying VMS-hosting rhyolites (Davis et al. 1985; Bailes et al. 1996; Barrett and MacLean 1999) and have U–Pb zircon ages which indicate they are broadly coeval with their enveloping volcanic successions (Davis et al. 1985; Mortensen 1993; Bailes and Galley 1999; Galley et al. 2000).

The physical aspects of these four intrusive complexes will be used to define some of the characteristics of magmatic bodies which intrude to a sufficiently shallow level below the seafloor to initiate and sustain a robust, hydrothermal convection system. Their primary geochemical character defines the type of tectonic environment in which they developed, and shows why these environments are optimal for the generation of VMS camps. The presence of distinctive alteration assemblages is further evidence of their interaction with seawater at shallow crustal levels.

Intrusion-VMS relationship: hypothesis

The premise for the relationship between subseafloor intrusions and VMS deposits is that the high-level (< 1 kbar) emplacement of a magma chamber beneath the seafloor heats up connate seawater within relatively permeable, seafloor volcanic and volcaniclastic strata (Fig. 3). The heated water forms an advection column upwards to the seafloor which in turn draws cold seawater into its flanks, resulting in a fluid convection system. As the seawater is drawn into the subseafloor, it becomes progressively hotter in relation to the elevated thermal gradient defined by the cooling intrusion. This results in a series of fluid-rock reactions during which progressively higher-temperature, secondary mineral assemblages form in the rocks. The mineralogical variation is accompanied by changes in major- and trace-element patterns as well as isotopic variations. These reactions cause the seawater to change in composition from a weakly alkaline, cold fluid to an acid, hot, reduced fluid capable of stripping and maintaining metals in solution, principally as chloride complexes (von Damm 1995). These hot (350–450 °C) fluids undergo a density decrease which allows them to rise buoyantly towards the seafloor. In the near-seafloor environment, the fluids are quenched with cold seawater and then precipitate sulfide minerals, silicates, sulfates and carbonates as massive sulfide lenses and associated, vein stockwork systems.

Evidence for the involvement of the high-level subvolcanic intrusions in convective hydrothermal systems

Table 1 List of known, probable, and possible, large (> 10 km²) subvolcanic intrusions associated with VMS camps

Pluton	Age (Ma)	Location	Rock type[a]	Intrusion type	Composition	Area (km²)	Associated volcanics	Associated mineralization[b]	Aggregate tonnage (t)	Reference
Mafic(-ultramafic)										
Pike Lake[c]	2,735	Ignace, ON	An-Gb	Layered mafic	Th–Cc	20	South Sturgeon	VMS occurrences	–	Trowell (1974)
Lac Dore	2,728	Chibougamau, QC	Gb–An–Gran	Layered mafic	Th	800	Waconichi	2 VMS	3.7	Allard (1976)
Bad Vermillion[c]	2,727	Mine Centre, ON	Gb–An–Gran	Layered mafic	Th	100	Keewatin	VMS occurrences	–	Ashwal et al. (1983), Poulsen and Hodgson (1984)
Bell River	2,724	Matagami, QC	Gb–An–Gran	Layered mafic	Th	700	Watson Lake	12 VMS	40	Maier et al. (1996)
Kamiskotia	2,707	Timmins, QC	Gb	Layered mafic	Th	180	Kamiskotia	3 VMS	8	Barrie and Davis (1990)
Tonalite–trondhjemite										
Chester	2,740	Swayze, ON	QD–Tn–Tr	Composite	Th–Cc	100	Chester	Iron formation	–	Ames et al. (1997)
Biedelman Bay[d]	2,735	Ignace, ON	QD–Tn–Tr	Composite	Th–Cc	30	South Sturgeon	4 VMS, 1 Cu–Mo	35	Trowell (1974), Poulsen and Franklin (1981), this study
Brouillan	2,729	Selbaie, QC	Tn–Grdt–Grnt	Composite	Cc	500	Hurricana-Turgeon	1 VMS	22	Barrie and Krogh (1996)
Mud Lake[d]	2,727	Mine Centre, ON	Tn–Tr	Composite	Th	30	Keewatin	13 VMS	–	Ashwal et al. (1983), Poulsen and Hodgson (1984)
Phinney-Dash	2,727	Kenora, ON	Tn–Tr	Composite	Cc	20	Katimiagamak	VMS occurrences	–	Hodder (1981)
Geco	2,720	Manitouwadge, ON	Tr–Grdt–Grnt	Composite	Th	50	Manitouwadge	4 VMS	60	Zaleski and Peterson (1995)
Flavrian-Powell	2,701	Rouyn, QC	QD–Tn–Tr	Composite	Th	50	Blake River	17 VMS, 2 Cu–Mo	110	Goldie (1976), Kennedy (1985), this study
Boulamaque	2,700	Val d'Or, QC	Drt–QD	Composite	Th	170	Val d'Or	3 VMS	50	Pilote et al. (1998)
Mooshla[d]	2,696	Bousquet, QC	QD–Tn–Tr	Composite	Cc	10	Blake River	1 VMS, 1 Au–Cu (Doyon)	54	Langshur (1991)
Clericy	2,696	Rouyn, QC	QD–Tn	Composite	Th	10	Blake River	1 VMS (Mobrun)	10	Trudel (1978), Mortensen (1993)
Anialik River	2,694	N. Slave, NWT	QD–Tn–Tr	Composite	Th	200	Anialik	6 VMS	–	Abraham et al. (1994)
Viterliden	1,890	Skellefte, Sweden	QD–Tn–Tr	Composite	Cc	25	Skellefte	3 VMS	30	Bergström et al. (1998)
Richard Lake	1,889	Snow Lake, MB	Tn–Tr	Composite	Th–Cc	20	Snow Lake	4 VMS	15	Bailes and Galley (1999), this study
Jorn	1,886	Skellefte, Sweden	Tn–Tr	Composite	Cc	150	Skellefte/Vargfors	4 VMS, Cu–Mo occurrence	27	Weihed (1992)
Sneath Lake	1,886	Snow Lake, MB	Tn–Tr	Composite	Th	30	Snow Lake	3 VMS	20	Bailes and Galley (1999), this study
Bald Mountain	458–445	Aroostock Cty, MN	Tn–Tr	Composite	Th	10	Winterville Fm.	1 VMS	30	Froose et al. (2002)
Mule Mountain[e]	400	West Shasta, CA	Tn–Tr	Composite	Th	45	Copely	13 VMS	16	Taylor and South (1985), Albers and Bain (1985)
Lasail	95	Semail ophiol., Oman	Tn–Tr	Composite	Th	5	VII-VIII	1 VMS	16	Alabaster and Pierce (1985)
Aarja	95	Semail ophiol., Oman	Tn–Tr	Composite	Th	5	VII-VIII	2 VMS	10	Haymon et al. (1989)
Probably related to VMS deposits										
Strelley[e]	3,237	Pilbara, W. Australia	Hb Grnt–K Grnt	Composite	Cc	220	Strelley	2 VMS	7	Brauhart et al. (1998)
Manyutup[e]	2,989	Yilgarn, W. Australia	Tn–Tr	Composite	Cc	128	Ravensthorpe	Cu–Au and VMS occurrences	–	Witt (1999)

Table 1 (Contd.)

Pluton	Age (Ma)	Location	Rock type[a]	Intrusion type	Composition	Area (km²)	Associated volcanics	Associated mineralization[b]	Aggregate tonnage (t)	Reference
Arkala	1,890 (?)	Pyhäsalmi, Finland	Tn–Tr	Composite	Th	24+	Pyhäsalmi	3 VMS	50	Weihed (1991)
Darwin-Murchinson	500	Tasmania, Australia	High-K Grnt	Composite	Cc	220	Mount Read	4 VMS	148	Large et al. (1996)
Palekhori	92	Cyprus	QD–Tn–Tr	Composite	Th	10	Troodos	3 VMS	10	Moore (1986)
Possibly related to VMS deposits										
Grassmoor Dome	1,250 (?)	South Africa	High-K Grnt	Granite gneiss	Cc	120	Areachap	2 VMS	50	Alldrick (1978)
Mt. Morgan	381	Queensland, Australia	QD–Tn–Tr	Composite	Cc	50	Mount Morgan	1 VMS	50	Messenger and Golding (1996)
Campofrio[e]		Spain	Tn–Tr	Composite	Cc	200	Iberian Pyrite Belt			Schutz et al. (1987), Stein et al. (1996)

[a] An, Anorthosite; Drt, diorite; QD, quartz diorite; Gran, granophyre; Gb, gabbro; Grnt, granite; Grdt, granodiorite; Hb, hornblende; Tn, tonalite; Tr, trondhjemite; Th, tholeiite; Cc, calc-alkaline
[b] Does not include orogenic deposits
[c] Mafic layered intrusion associated with a coeval composite intrusion
[d] Composite intrusion associated with coeval mafic layered intrusion
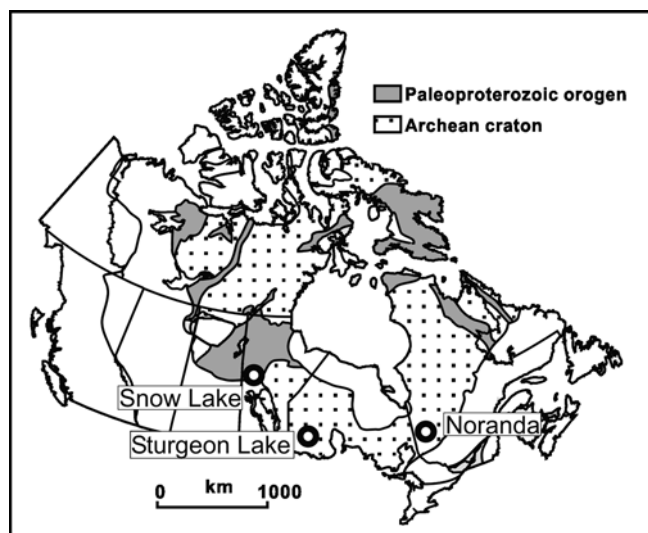[e] Probably undergone structural thickening through thrusting

Fig. 1 Location of the studied Precambrian VMS camps, Canada

includes the presence of fracture-controlled, 350–450 °C secondary mineral assemblages within the intrusions (Mével and Cannat 1991; Kelley and Gillis 1993; Gillis et al. 1993; Nehlig 1993). These altered and mineralized fractures are believed to represent "cracking fronts" formed by the circulation of hydrothermal fluid during thermal contraction of the cooling margin of the intrusion (Lister 1972; Cathles 1983). Subvolcanic intrusions in modern, spreading ridge environments, ophiolites and ancient arcs also show isotopic evidence for interaction with hot, evolved seawater (Gregory and Taylor 1981; Stakes and Taylor 1992; Cathles 1993).

Physical descriptions

The physical characteristics of composite synvolcanic intrusions associated with VMS camps are important for two reasons. Recognition of distinctive field relationships allows the explorationist to quickly evaluate the potential for an intrusion to have been involved in the generation of a VMS-related, subseafloor hydrothermal system. These characteristics are also important in allowing more precise, thermal modeling of subvolcanic systems and to ascertain which conditions are necessary for initiation of convective hydrothermal activity.

Beidelman Bay Intrusion

The 18-km-long BBIC intruded the top of a pre-cauldron basalt succession which underlies the felsic, pyroclastic, rock-dominated 2,735-Ma Sturgeon Lake cauldron, host to five Zn–Pb–Cu VMS deposits (Morton et al. 1990; Fig. 2A). The volcanic rocks and associated subvolcanic intrusions are part of the South Sturgeon volcanic belt of the Superior Wabigoon subprovince (Sanborn-Barrie et al. 2001). The F Group and Mattabi
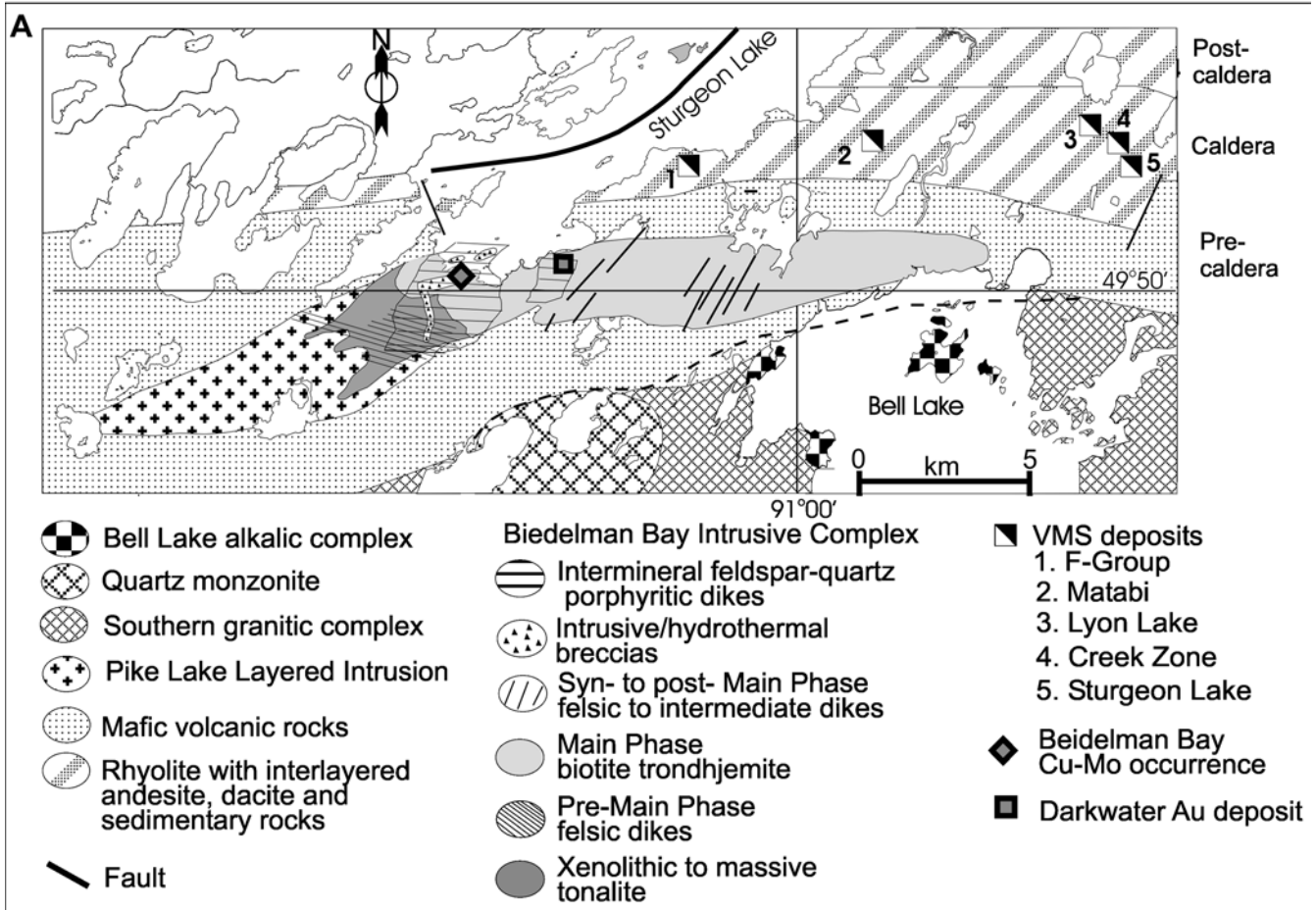
Fig. 2 Geology of the **A** BBIC within the Archean Sturgeon Lake VMS camp, **B** the FPIC within the Archean Noranda VMS camp, and **C** the SLIC and RLIC within the Paleoproterozoic Snow Lake VMS camp. The geology of the BBIC is modified after Trowell (1974), that of the Sturgeon Lake camp after Morton et al. (1990), that of the FPIC after Kennedy (1985), and that of the Noranda camp after Gibson and Watkinson (1990). The geology of the SLIC and the Snow Lake VMS camp is extracted from Bailes and Galley (1999)

VMS deposits directly overlie the BBIC whereas the Sturgeon, Lyon and Creek Zone deposits are hosted in overlying volcanic strata 2 km east of the composite intrusion.
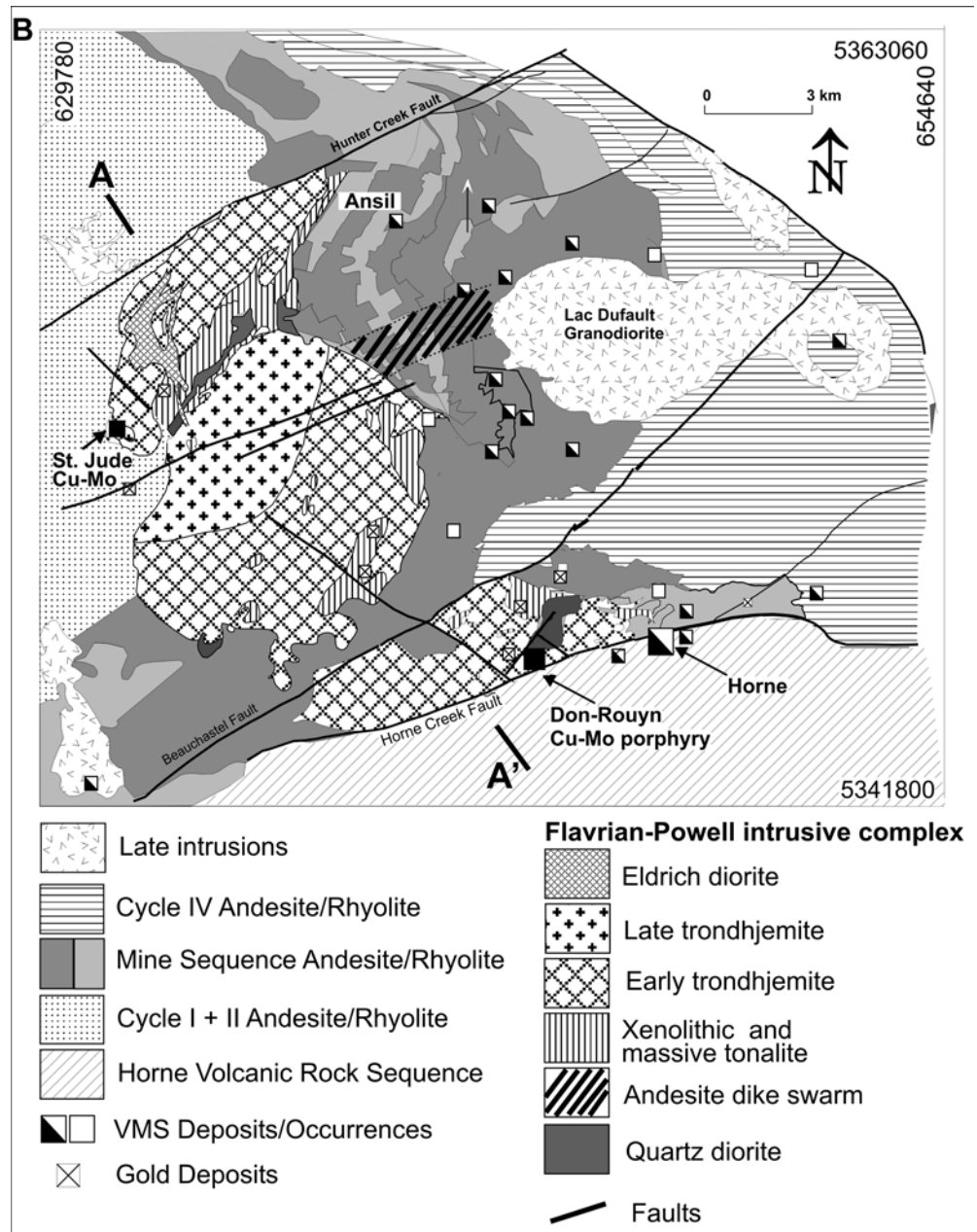
The BBIC is poorly exposed over much of its strike length, with only a few outcrops of the early phases of the intrusions. The earliest phase appears along the eastern end of the BBIC and consists of sheets as thick as 150 m of xenolithic quartz diorite which intrude the 2,733 + 6/−3 Ma Pike Lake mafic layered intrusion (Fig. 2A). The xenoliths are dominantly the melano-gabbro wall rocks. The xenolithic quartz diorite likely represents about 5–10 vol% of the BBIC. It is cut by an aphyric tonalite which is densely xenolithic along some of its margins. It appears to have been emplaced as a series of sills which are as much as 300 m thick over a 2,000-m stratigraphic interval, with individual sills separated by remnants of the Pike Lake intrusion and the

earlier BBIC quartz-diorite phase. The remnant of the tonalite sill complex represents approximately 15–20 vol% of the BBIC. It is approximately 5 km in strike length, cut by a swarm of quartz porphyry trondhjemite dikes and truncated to the east by a series of comagmatic hornblende-biotite- and biotite-bearing trondhjemites. The trondhjemites form the bulk (70–80 vol%) of the BBIC, as a sill complex 15 km long and as much as 2,700 m thick. They contain a number of internal contacts which vary from sharp, chilled margins to more gradational contacts marked by broader grain-size variations. None of these contacts can be followed for any distance, which suggests they were disrupted by sequential injections of trondhjemitic magma. The phases change from a hornblende-biotite- to a biotite-bearing variant as the sill thickens to the east.

The trondhjemite phase has a U–Pb zircon date of 2,734 Ma (Davis et al. 1985). It is similar in age and composition to the Middle "L" pyroclastic flows in the upper part of the cauldron complex (Galley et al. 2000). At 2,715 Ma, the BBIC was transected by quartz-feldspar porphyritic granodiorite dikes and associated Cu-Mo-bearing, intrusive-hydrothermal breccias temporally associated with post-cauldron, felsic volcanic rocks (Poulsen and Franklin 1981; Galley et al. 2000).

Subsequent deformation tilted the composite intrusion steeply to the north and imprinted the rocks with a

Fig. 2 (Contd.)

B

Hunter Creek Fault

Ansil

Lac Dufault
Granodiorite

St. Jude
Cu-Mo

Horne

Don-Rouyn
Cu-Mo porphyry

Beauchastel Fault

Horne Creek Fault

5363060

654640

0   3 km

N

5341800

629780

A

A'

Legend:

Late intrusions

Cycle IV Andesite/Rhyolite

Mine Sequence Andesite/Rhyolite

Cycle I + II Andesite/Rhyolite

Horne Volcanic Rock Sequence

VMS Deposits/Occurrences

Gold Deposits

Flavrian-Powell intrusive complex

Eldrich diorite

Late trondhjemite

Early trondhjemite

Xenolithic and massive tonalite

Andesite dike swarm

Quartz diorite

Faults

strong, subvertical ENE schistosity which overprints much of the primary texture. The intrusion is bordered to the south, and offset by a number of late kinematic shear and fault zones. The major crosscutting fault contains shear-zone-hosted subeconomic gold mineralization (Poulsen and Franklin 1981). A biotite–chlorite regional metamorphic isograd bisects the BBIC along its long axis.

Flavrian-Powell Intrusion

The 15-km-long FPIC intrudes the base of the approximately 2,701–2,698 Ma bimodal basalt- and rhyolite-infilled Noranda cauldron which is host to 17 Zn–Cu

VMS deposits, including the 54-Mt Horne deposit (Gibson and Watkinson 1990; Mortensen 1993; Fig. 2B). The cauldron succession is part of the Blake River Group in the Southern Abitibi greenstone belt, Superior subprovince, and has a 35-km strike length (Peloquin et al. 1990; Hannington et al. 2002, this volume).

The earliest phase presently comprises approximately 10 vol% of the FPIC as pendants and xenoliths of fine-grained, aphyric quartz diorite in later tonalite and trondhjemite phases. It appears to have formed as a series of quartz-diorite sills and dikes which intruded into the top of a basaltic volcano along the lower contact of the cauldron. This early sill complex is centered about quartz-diorite dike swarms which define two eruptive centers within the Noranda cauldron (Gibson and
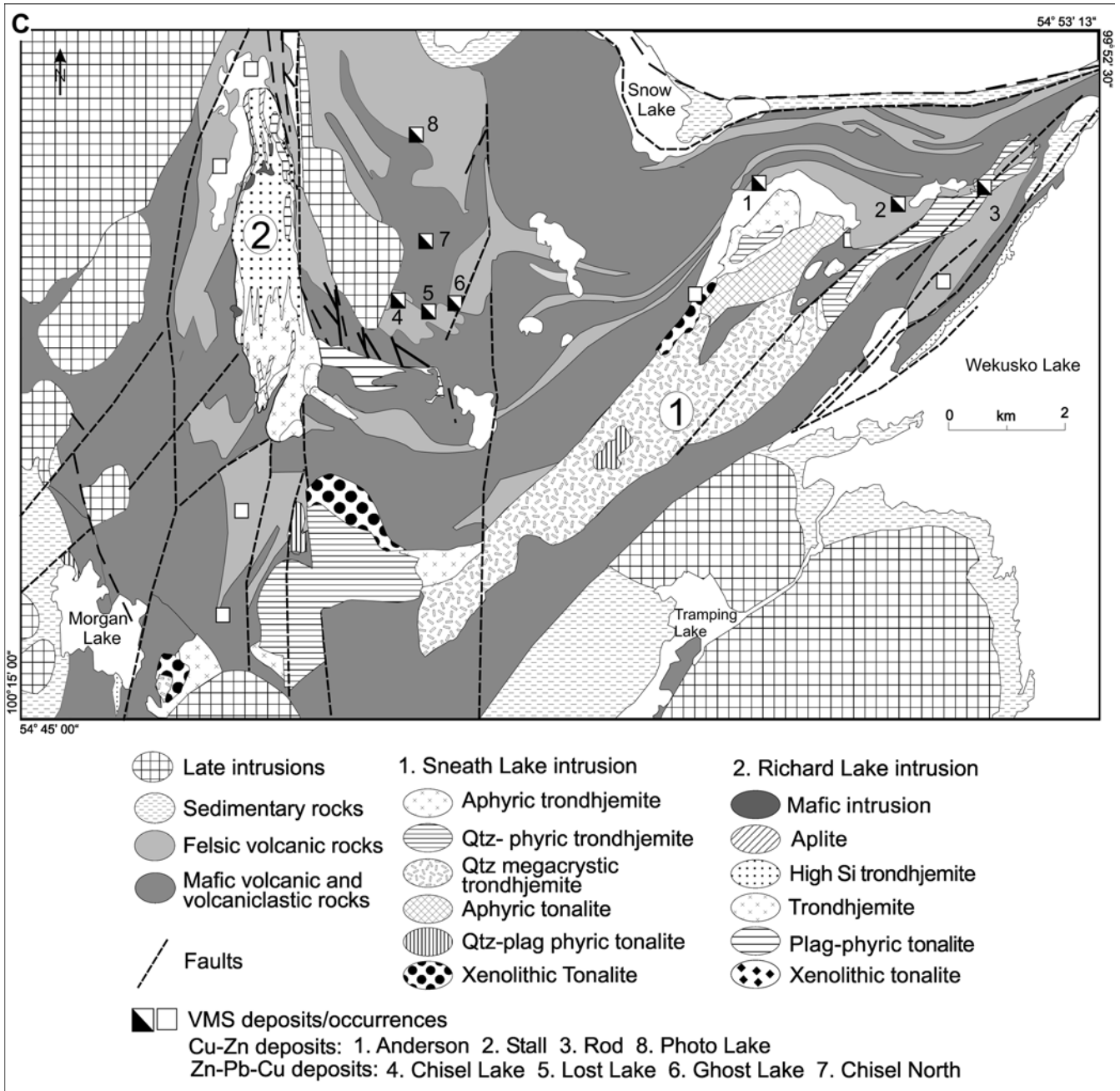
Fig. 2 (Contd.)

Watkinson 1990). The dike swarms were the feeder systems for much of the basaltic andesite which infilled much of the cauldron (Gibson 1989; Gibson and Watkinson 1990).

The tonalite phase now comprises approximately 20 vol% of the FPIC as pendants and xenoliths in successive trondhjemite phases. It includes xenolithic, "hybrid" and massive facies (Goldie 1978). The xenolithic facies contain as much as 60% angular to lobate xenoliths of basalt, quartz diorite and tonalite. The hybrid facies contain partially absorbed, amoeboid blebs of mafic rock and lobate blocks of trondhjemite (Fig. 4A).

The contacts between the pendants of quartz diorite and hybrid tonalite can have gradational contacts over tens of meters, in which the quartz diorite acquires abundant, 3–6 mm diameter, zoned quartz–amphibole–feldspar ovoids (pseudophenocrysts) and the tonalite-abundant dendritic amphibole (Fig. 4A). The massive, fine-grained aphyric tonalite can contain 10–15% dendritic pyroxene–amphibole which are as much as to 20 mm in length. Miarolitic cavities, 5 to 15 mm in diameter, are infilled with amphibole, quartz, chlorite and epidote (Fig. 4B). These cavities are particularly abundant within the xenolithic tonalite.
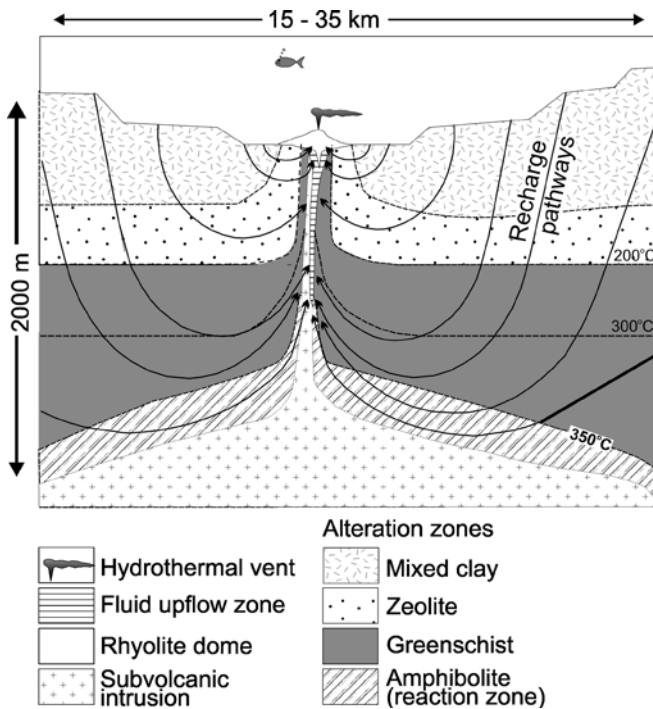
Fig. 3 A conceptual model for the formation of a VMS deposit through a hydrothermal system dominated by subseafloor seawater convection initiated and sustained by a shallowly emplaced subvolcanic intrusion (modified after Galley 1993). The semiconformable, hydrothermal alteration facies form because of interaction between convecting seawater and rocks at ever-increasing temperatures approaching the subvolcanic intrusion. Spooner and Fyfe (1973) defined these zones using metamorphic terminology because of the mineralogical resemblance of these subseafloor alteration zones to regional metamorphic mineral assemblages

The tonalite represents the product of a relatively closed magma system. The only evidence for a volcanic rock equivalent within the Noranda cauldron is a small dacite flow associated with the Ansil VMS deposit in the lower half of the cauldron (Galley 1994).

The 2,701-Ma trondhjemite phases of the FPIC comprise 65–70 vol% of the composite intrusion emplaced in two main stages (Kennedy 1985; Mortensen 1993). The early trondhjemite occurs as a series of composite sills which are tens of meters thick and interlayered with xenolithic to massive tonalite and xenolithic trondhjemite of similar thickness. Contacts between these three units are sharp to gradational over centimeters. Contacts are also sharp between the quartz-diorite phase and dikes of early trondhjemite. The xenolithic trondhjemite contains subrounded to subangular xenoliths of quartz diorite and tonalite which have sharp to pegmatitic, recrystallized margins (Fig. 4C). This early trondhjemite is fine to medium grained, with textures which range from equigranular to weakly quartz phyric and spherulitic (Fig. 4D). The massive trondhjemite sills contain columnar joints in places. The emplacement of the trondhjemite was accompanied by intrusion of numerous trondhjemite–rhyolite dikes into the overlying volcanic strata. Many of these dikes are

demonstrated to be feeders for late- to post-cauldron rhyolite flows (Setterfield et al. 1995).

Miarolitic cavities are common in both tonalite and trondhjemite but are most abundant within the xenolithic facies of both. The cavities range from millimeters to centimeters in diameter, the larger ones commonly having epidotized or silicified, aplitic halos as much as several centimeters in width (Fig. 4B). In some cases, cavities have high aspect ratios and resemble large pipe vesicles which can extend for several meters (Fig. 4F). Along with fracture- and vein-controlled alteration, the mineral assemblages which infill the cavities indicate that these early intrusive phases are affected by hydrothermal-magmatic and hydrothermal alteration. This will be discussed in a following section.

The 2,701-Ma, early trondhjemite phase is cut by several discontinuous, irregularly shaped bodies known as the Eldrich diorite (Goldie 1976; Mortensen 1993). These mafic stocks have scalloped contacts with the early trondhjemite, indicating their intrusion into a still-plastic host (Castro et al. 1990; Fig. 4E).

The Eldrich diorite is in turn intruded by a 2,701-Ma, late trondhjemite phase which now cores the FPIC (Kennedy 1985; Galley and van Breemen 2002). The late trondhjemite has sharp, brecciated contacts with the earlier intrusive phases, and contains 15–20% rounded xenoliths of mafic volcanic quartz diorite, tonalite and early trondhjemite. Its contacts appear semiconformable to discordant with the older FPIC phases, suggesting intrusion as a sill-stock complex. The lack of fracture, vein or miarolitic cavity-controlled alteration within the late trondhjemite suggests that it postdates the seafloor hydrothermal activity which affects the earlier phases (Kennedy 1985). This is supported by oxygen isotope evidence (Kennedy 1985; Cathles 1993; Taylor and Holk 1998). This places a very tight constraint on the duration of the VMS hydrothermal event, as both the early and late trondhjemite phases of the FPIC have similar ages. There are several reasons to believe the late trondhjemite was the focus of magmatic-related mineralization and alteration. It has a halo of ferroactinolite–biotite–apatite–sulfide veins suggestive of volatile exsolution and fluid migration during crystallization. A small stock of late trondhjemite cores a 600-m-diameter St. Jude intrusive breccia pipe with a Mo–Cu mineralized core and peripheral Zn–Pb–Ag veins emplaced before 2,697 Ma (Kennedy 1985; Carriere 1992; Galley and van Breemen 2002; Fig. 2B).

The FPIC and host volcanic strata have been affected by regional deformation and lower greenschist metamorphism. They underwent homoclinal folding which tilted the rocks 20 to 45° to the east. The apparent dislocation of the northern 75% of the FPIC from the southern 25% (Fig. 2B) is due to north-verging thrusting (Richards 1999). This was followed by truncation of the north and south margins of the FPIC by further faulting, including the development of several, large shear-fault zones which are host to five orogenic gold deposits (Kennedy 1985; Richards 1999).

Fig. 4 A Partly absorbed blebs of quartz diorite within a tonalite host of the Flavrian-Powell composite intrusion. Note the dendritic amphibole crystals (*circle*) within the tonalite which are a result of disequilibrium crystallization. **B** FPIC trondhjemite containing numerous miarolitic cavities infilled with epidote and quartz and surrounded by epidosite halos (4-cm coin for scale). **C** FPIC tonalite xenoliths within early trondhjemite phase. Note the pegmatitic margins on the xenoliths. **D** Coarsely spherulitic FPIC trondhjemite with spherulites surrounded by epidote-chlorite-amphibole-rich areas (4-cm coin for scale). **E** Scalloped contact between the early-phase FPIC trondhjemite and the Eldrich diorite. Note chilled margin on the trondhjemite, and back-diking of the trondhjemite into the younger diorite. There is no alteration of the Eldrich diorite, as opposed to the strongly altered nature of the early quartz diorite (4-cm coin for scale). **F** Epidote-filled miarolitic pipe vesicles infilled with strongly silicified margins within the FPIC early trondhjemite phase (12-cm-long pen for scale). **G** Xenolithic tonalite phase to the SLIC with closely packed fragments of basalt and gabbro of varying texture and grain size (35-cm-long hammer for scale). **H** Well-developed columnar joints within a phase of SLIC trondhjemite. Note bleached margins which denote fracture-controlled hydrothermal alteration
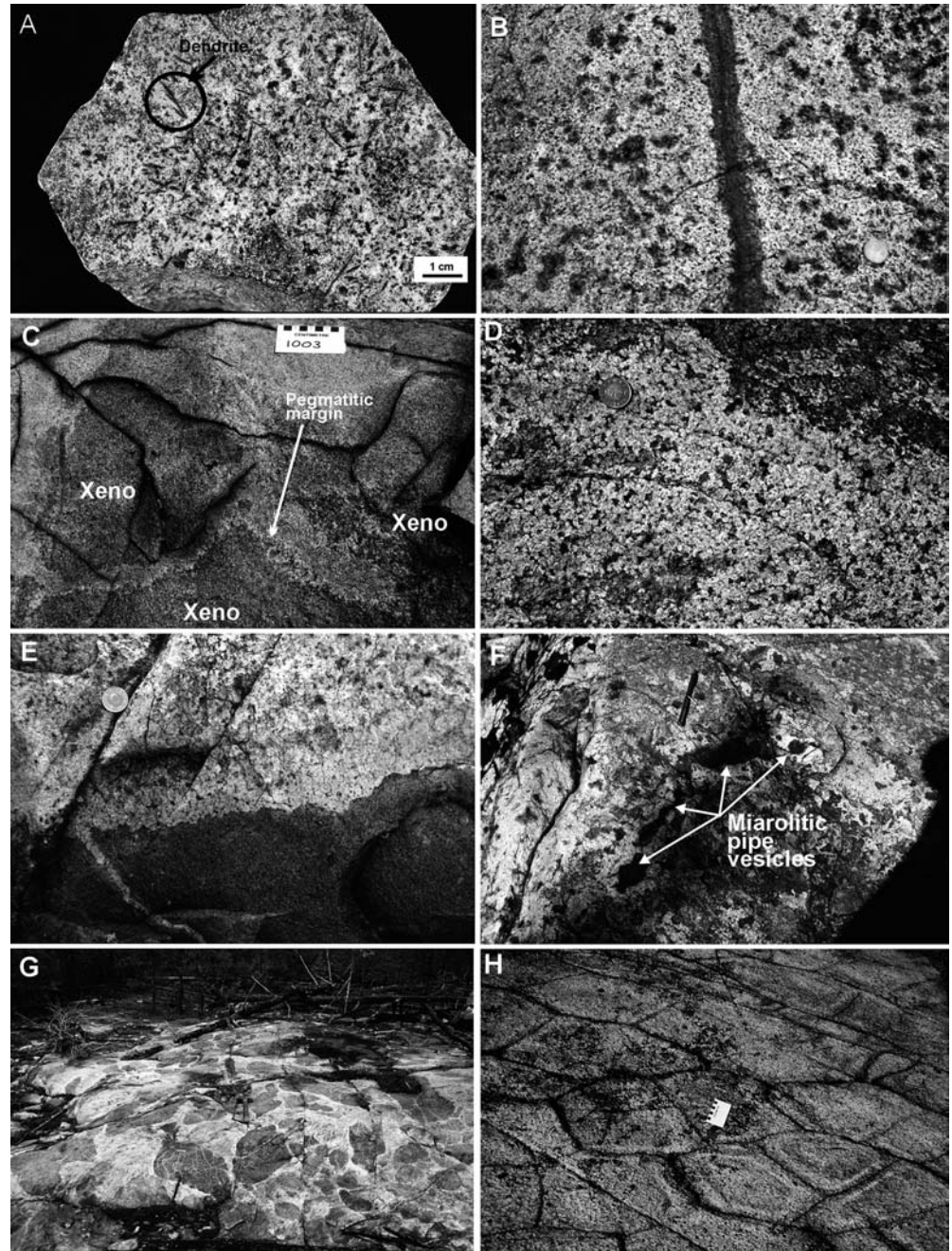
Sneath Lake Intrusion

The SLIC is hosted within a bimodal, flow-dominated basalt–rhyolite volcanic rock succession within the lowermost Snow Lake arc assemblage of the Flin Flon greenstone belt, which forms part of the Paleoproterozoic Trans-Hudson Orogen. Two rhyolite flow complexes in the volcanic succession overlying the SLIC are comagmatic with the composite intrusion, and contain three Cu–Zn–Au VMS deposits and five large VMS occurrences (Fig. 2C).

The composite intrusion is 18 km long and as much as 2,500 m thick, with an average thickness between 1,000 and 1,500 m (Fig. 2C). There is an asymmetric distribution of internal phases which proliferate within the two ends of the intrusion. Remnants of equigranular, massive to xenolithic tonalite occur along the upper contact of the SLIC. They contain angular to subrounded xenoliths as much as 2 m in length, comprised of amphibolite, gabbro and quartz diorite (Fig. 4G). The xenoliths are the only evidence that there may have been an early mafic phase to the composite intrusion. The tonalite is characterized by as much as 15% actinolitic hornblende. The restriction in distribution of the tonalite phases to either end of the SLIC suggests their emplacement as stocks or small sills directly below

a volcanic eruptive center. This conclusion is supported by the fact that the two largest rhyolite flow complexes within the volcanic host rock lie directly above the two ends of the composite intrusion (Fig. 2C).

A series of hornblende-biotite- to biotite-bearing trondhjemite stocks overprints the tonalite at the two ends of the composite intrusion. A number of quartz phyric trondhjemite stocks are enveloped by at least two pulses of quartz megacrystic trondhjemite. At the western end of the SLIC, the quartz phyric stocks remain as pendants within the first phases of quartz megacrystic trondhjemite. The western margin of this body contains well-developed columnar joints (Fig. 4H). The second quartz megacrystic phase occupies the core of the SLIC as a 5-km-long by up to 2,000-m-thick sill. Sharp-sided dikes of the quartz megacrystic trondhjemite cut the tonalite phases formed earlier, but contacts between the different trondhjemite phases are gradational over centimeters to tens of meters. Convincing evidence that the central, quartz megacrystic sill is younger than the quartz phyric stocks is the presence of altered pendants of the latter in the unaltered former.

At the eastern end of the SLIC, a quartz phyric trondhjemite stock transects all previous phases and intrudes the overlying rhyolite complex and envelops the rhyolite-hosted Rod VMS deposit (Fig. 2C). Dikes associated with this phase intrude into the basaltic andesite overlying the VMS-hosting rhyolite complex. There are several small, late quartz-plagioclase porphyry stocks within the SLIC which are comagmatic with the next cycle of volcanism (Bailes and Galley 1999). Both ends of the SLIC are transected by mafic dike swarms which are comagmatic with basaltic flows in younger volcanic rock successions.

The rocks in the Snow Lake arc assemblage are poorly dated due to low high-field-strength element (HFSE) concentrations (Stern et al. 1995). A discordant U–Pb zircon date of 1,986 Ma is reported for the SLIC (Bailes et al. 1996). The only U–Pb date from the host volcanic rock succession comes from a quartz megacrystic trondhjemite clast within a felsic breccia at 1,892 Ma (David et al. 1996). The clast is texturally and compositionally identical to the quartz megacrystic phase of the SLIC.

At the cessation of synvolcanic magmatism, the SLIC and enclosing strata were folded during two phases of deformation during which a strong east to northeast schistosity developed which has overprinted many of the primary textural features of the composite intrusion. The composite intrusion is affected by biotite–garnet facies regional metamorphism.

Richard Lake Intrusion

The RLIC forms part of the second volcanic cycle of the Snow Lake arc assemblage (Fig. 2C). The enclosing rocks include basalt flows overlain by a fractionated basalt–andesite–dacite–rhyolite succession with a large component of volcaniclastic and epiclastic formations. One Cu–Zn–Au and four Zn–Pb–Cu–Ag–Au VMS deposits lie within rhyolite flow complexes at the top of the volcanic cycle.

The RLIC has a morphology different from the other three, sill-like composite intrusions. It is a composite stock approximately 6,500 m in height, as much as 3,000 m wide, and with an average width of about 1,000 m (Fig. 2C). The earliest RLIC-related intrusive phase consists of remnants of small stocks of hornblende porphyritic diorite preserved along the margins of the composite intrusion, and as xenoliths within early tonalite phases. They are compositionally similar to andesite flows within the host volcanic rock succession (Bailes et al. 1996). The next phase occurs as a 2-km-long, feldspar porphyritic dacite–tonalite sill-dike complex which intruded along the top of the basal basalt flow formation and at the base of a turbidite-debris flow succession. The dacite dikes reach upsection for nearly 1,000 m as feeders for a dacite volcanic formation which defines the immediate foot wall to the VMS-hosting, rhyolite flow complexes. The composite sill is ≤ 300 m wide and thins to the east as it bifurcates into a number of thinner sills. It is truncated to the west by later trondhjemitic phases of the RLIC. The presence of tonalite as infilling between pillows in basalt flows along the southern contact of the RLIC suggests a feeder zone for the dacite–tonalite sill-dike swarm.

The main portion of the RLIC consists of a number of overlapping biotite trondhjemite and aplite stocks and dikes. Contacts are not commonly observed but rapid textural changes and phenocryst populations suggest many are gradational. The southern (lower) half of the intrusion contains small bodies of medium- to coarse-grained, equigranular trondhjemite within a larger stock of finer-grained, quartz phyric trondhjemite. The quartz phyric trondhjemite stock is in turn intruded by dikes of aphyric to weakly quartz phyric, holocrystalline to granophyric trondhjemite. The dikes coalesce into a composite stock in the middle of the RLIC. The composite stock bifurcates into a series of dikes in the upper third of the intrusive complex. The dikes of this third trondhjemite phase are not observed cutting the bodies of coarse-grained trondhjemite. The dikes of the third-phase trondhjemite in the northern (upper) half cut domains of hornblende gabbro and aphyric to xenolithic hornblende tonalite. The trondhjemite phases are characterized by abundant miarolitic cavities which range from < 10 mm in size near the margins of the intrusive complex to ovoids ≤ 15 cm in diameter. Some miarolitic cavities are elongate and form epidote-quartz-infilled bubble "trains", particularly along the margins of aplite dikes.

Sparsely-quartz-phyric aplite dikes transect the trondhjemite and tonalite phases in the upper two thirds of the RLIC. They can be several centimeters to tens of meters wide and strike north along the axis of the composite intrusion. They are commonly granophyric and hematite-stained. The last dike phase consists of

aphyric to plagioclase, porphyritic mafic dikes. They are as wide as several meters, have cuspate, irregular margins, can be segmented in places and, at times, terminate within the trondhjemite host rocks. As with the late mafic dikes which transect the SLIC, these dikes are compositionally similar to basalt flows in the succeeding volcanic cycle.

A single U–Pb zircon date from a coarse-grained trondhjemite phase gives an age of 1,889 Ma for the RLIC (Bailes et al. 1991). There are no age determinations for the host volcanic rocks but the geological and geochemical relationships between the early dacite–tonalite sill-dike complex and overlying dacitic volcanic rocks suggest that at least the early phases of the RLIC are comagmatic and coeval with their host rocks.

After the cessation of magmatic activity, the RLIC was affected by two phases of folding and offset by a series of late, north-trending faults. The rocks are overprinted by biotite–garnet facies regional metamorphism.

Intrusion compositions

Close to 300 samples were collected for geochemical analysis. Each of these samples has an accompanying, polished thin section which was used for detailed petrographic examination. Of these, 130 were considered least altered and suitable for use in identification of primary compositions and as petrologic discriminates. The remainder are used to reconstruct the alteration history of each intrusive complex. Analyses were carried out by the Analytical Laboratories at the Geological Survey of Canada, using XRF wavelength dispersive analysis on fused disks, and ICP-MS and ICP-ES on powders for major-, trace-, and rare-earth elements. Iron oxide, $H_2O_{(t)}$, $CO_{2(t)}$, and $S_{(t)}$ were analyzed by chemical methods, and Pb and Ag by atomic absorption spectrometry. Fluorine and chlorine analyses were determined using a Dionex anion chromatography analyzer. Information on the detection limits and accuracy for all these methods is available at http://www.132.156.95.172.

Due to the large size of the geochemical database, only a selected number of analyses is presented in this paper (Table 2). The complete data set is available from the Springer server http://link.springer.de for subscribers, or from the author upon request.

An understanding of the mineralogical and geochemical characteristics of Precambrian, VMS-related composite intrusions is essential in distinguishing them from more evolved magmatic suites not commonly related to subseafloor hydrothermal systems. Their geochemical signatures are also useful as petrogenetic indicators to determine the type of arc environments most amenable to the development of productive VMS camps. For the purpose of this understanding, a selected number of samples was chosen from each intrusive complex as examples of least-altered compositions (Table 2).

Mineralogy

The magmatic suites represented by the four subvolcanic intrusive complexes have a relatively primitive mineralogy. The more melanocratic phases consist of actinolitic hornblende (>20%), plagioclase (50–60%), quartz (5–20%), magnetite, and apatite with secondary biotite, chlorite, epidote, albite, titanite and carbonate. Remnants of pyroxene crystals are observed in the FPIC (Goldie 1976) and BBIC. The leucocratic phases consist of plagioclase (40–60%) and quartz (20–40%), along with lesser amounts of green amphibole (<2%), biotite (<5%) and magnetite, and accessory apatite, zircon, pyrite, chalcopyrite, pyrrhotite and perthite. Secondary minerals include ferroactinolite, epidote, chlorite, sericite, magnetite, titanite, albite, garnet, staurolite and kyanite. Plagioclase ranges from andesine to albite, with albite–oligoclase and albite prevalent in the trondhjemite phases.

Geochemistry

Mesonormative mineral plots indicate that the majority of phases in all of the intrusive complexes are tonalite and trondhjemite (Fig. 5A, B), with a large number of high-silica (>74% SiO_2) trondhjemites (Fig. 5B, C). The four suites are characterized by high sodium (4–5%), low potassium (0.2–1%), and low aluminum (<14.5% for >70% SiO_2; Fig. 5D, E). On a normative ($Na_2O + K_2O$)–$FeO_{(t)}$–MgO ternary plot, the intrusive suites display a dominantly tholeiitic character (Fig. 5F). The exception is the SLIC, whose more magnesian compositions may be a function of a pervasive magnesian-metasomatism which appears to have affected much of the Snow Lake VMS-bearing volcanic assemblage. The tholeiitic nature of the suites is again apparent in the normative alkali feldspar–quartz–plagioclase ternary plot (Fig. 5B). In this plot, tonalite and low-silica trondhjemite samples from all four suites follow a tholeiitic trend, whereas the high-silica trondhjemites fall within and about the crustal melt field, as defined by Lameyre (1987).

Primitive-mantle-normalized spider plots of the rare-earth elements (REEs) and HFSEs for the four subvolcanic intrusive complexes indicate both similarities and differences (Fig. 6A–D). All of the suites have low normalized titanium and scantium values typical of felsic granitoid rocks in which oxides and pyroxene remain in the restite during the partial melting/fractionation process. The SLIC has the flattest $(La/YB)_N$ profile, which suggests it has the most primitive composition (Table 2). The relatively low niobium and zirconium concentrations for the SLIC are due to the generally low HFSE concentrations in all of the Snow Lake arc assemblage rocks. This is believed to reflect a strongly depleted source region (Stern et al. 1995). The FPIC has the next most primitive composition, with slightly elevated LREE and flat $(Gd/Yb)_N$ typical of transitional

Table 2 Selected geochemical analyses for the Beidelman Bay, Flavrian-Powell, Sneath Lake and Richard Lake synvolcanic composite intrusions. The samples are representative of least-altered, primary igneous compositions for the principal rock types within each intrusive complex

Sample	Beidelman Bay								Flavrian-Powell							Sneath Lake								Richard Lake								
	GIA-303-1	GIA-308-1	GIA-303-2	GIA-304-1	GIA-353-1	GIA-373-1	GIA-377-1	GIA-444-1	GIA-437-1	GIA-031-3	GIA-034-1	GIA-443-1	GIA-427-1	GIA-416-3	GIA-433-1	GIA-240-1	3404	7203	3073	GIA-243-1	GIA-219-2	GIA-200-1	GIA-205-1	GIA-136-1	GIA-135-2	GIA-137-1	GIA-101-1	GIA-063-1	GIA-091-1	GIA-130-1	GIA-060-1	GIA-095-2
SiO_2	54.7	64.7	71.2	76.9	77.3	78.1	78.1	53.3	68.0	68.4	71.2	71.7	74.4	75.6	76.9	71.9	73.6	73.8	74.4	75.4	76.1	76.7	78.3	63.5	64.0	69.4	72.3	72.7	74.6	74.9	75.7	77.2
TiO_2	0.88	0.87	0.64	0.17	0.19	0.19	0.18	1.06	0.54	0.25	0.33	0.33	0.29	0.35	0.14	0.27	0.20	0.24	0.20	0.22	0.11	0.21	0.19	0.56	0.53	0.30	0.25	0.30	0.24	0.25	0.21	0.12
Al_2O_3	16.8	14.8	13.1	11.5	11.3	11.3	11.4	17.0	13.5	15.80	14.1	13.1	12.7	12.2	11.4	13.3	12.5	13.6	12.2	12.4	12.0	10.6	11.8	13.9	14.2	12.7	12.3	12.4	12.1	11.8	11.7	11.9
$Fe_2O_{3(t)}$	10.8	5.2	5.6	2.8	1.6	1.6	2.2	10.6	8.0	4.2	5.0	5.1	2.1	3.8	2.7	4.5	4.8	2.0	4.3	4.1	3.1	5.4	1.8	10.3	10.3	7.1	10.4	6.2	6.4	5.9	3.8	3.1
Fe_2O_3	3.4	1.9	2.6	0.4	0.6	0.9	0.4		2.7	1.5	0.8	1.7	0.8	1.2	0.6	3.3	0.90	–	1.50	1.6	1.0	1.3	0.3	2.5	4.2	2.4	6.1	1.8	2.1	1.4	1.8	2.0
FeO	6.7	3.0	2.7	2.2	1.0	0.7	1.6	8.1	4.7	2.4	3.8	3.0	1.2	2.3	1.9	–	–	–	–	2.3	1.9	3.7	1.4	7.1	5.5	4.3	3.9	4.0	3.8	4.2	1.8	1.0
MnO	0.13	0.09	0.05	0.02	0.02	0.02	0.02	0.12	0.15	0.06	0.07	0.09	0.03	0.04	0.03	0.04	0.06	0.06	0.05	0.02	0.10	0.12	0.03	0.15	0.14	0.15	0.21	0.09	0.09	0.07	0.07	0.03
MgO	3.6	1.8	0.7	0.3	1.1	1.1	0.3	5.9	0.5	0.5	1.8	0.7	0.3	0.5	0.1	1.5	1.8	0.7	0.8	1.1	0.3	0.5	0.9	1.6	1.2	0.4	0.8	0.3	0.5	0.7	0.5	0.1
CaO	7.8	6.3	3.7	1.4	1.6	1.8	0.9	7.0	3.4	3.28	0.6	2.6	3.0	2.4	1.5	2.6	1.7	5.0	3.0	2.4	2.5	1.5	1.7	4.7	3.4	5.1	2.9	2.8	3.5	1.6	1.3	0.9
Na_2O	3.2	3.9	4.1	4.3	5.0	3.9	3.9	2.8	5.2	5.4	4.8	4.5	5.6	4.2	5.5	3.2	3.0	2.7	3.3	3.4	3.1	3.3	3.6	4.0	5.0	3.3	3.4	4.0	3.5	3.7	4.9	4.6
K_2O	0.9	0.3	0.2	0.9	0.7	1.0	1.5	0.1	0.3	0.9	0.5	0.5	0.2	0.5	0.3	0.9	1.6	0.5	0.7	1.0	0.8	1.0	0.8	0.9	0.7	0.9	1.5	1.0	1.2	1.0	0.7	1.7
H_2O	1.6	1.2	1.1	0.9	0.4	0.6	0.6	3.3	1.2	1.3	2.1	1.3	0.4	1.1	0.7	1.1	1.3	0.6	0.7	0.6	0.8	0.5	0.7	0.9	0.7	0.7	0.8	0.6	0.7	0.5	0.7	0.5
CO_2	0.2	0.6	0.0	1.0	0.9	0.2	<0.1	0.4	<0.1	0.1	0.4	<0.1	<0.1	<0.1	1.0	<0.1	0.70	0.70	2.0	<0.1	0.2	<0.1	0.2	0.2	0.4	0.3	0.2	<0.1	0.2	<0.1	0.05	0.07
P_2O_5	0.07	0.21	0.13	0.02	0.01	0.03	0.02	0.16	0.16	0.08	0.02	0.08	0.06	0.03	0.03	0.05	0.07	0.07	0.05	0.08	0.07	0.08	0.07	0.33	0.31	0.08	0.08	0.07	0.04	0.05	0.02	0.02
S	0.01	<0.01	<0.01	<0.01	<0.01	<0.01	0.02	0.03	<0.01	0.02	0.02	<0.01	<0.01	<0.01	<0.01	0.06	<0.01	<0.01	<0.01	<0.01	0.07	0.03	0.07	0.02	0.02	0.02	0.02	0.02	0.02	0.02	0.02	0.02
Total	100.1	99.7	100.3	99.9	99.2	99.3	99.0	100.8	100.4	101.0	99.7	99.7	99.0	100.3	100.1	99.1	95.7	99.7	95.0	100.5	98.8	99.5	100.0	100.3	100.3	100.1	104.6	100.2	100.7	100.1	100.3	100.7
Ba	230	130	130	220	190	190	390	93	250	215	161	210	240	200	210	250	346	100	229	280	200	230	90	450	80	490	330	560	510	240	200	650
Be	0.9	0.9	1.2	1.3	1.8	1.8	1.6	0.6	1.1	1.3	0.5	0.9	1.6	0.7	2	0.6	–	–	–	<0.5	<0.5	<0.5	<0.5	1.9	1.8	1.1	1.4	1.2	1.6	1.5	1.4	1.5
Co	25	<10	9	<10	<10	<10	<10	28	<10	16	15	<10	<10	<10	<10	<6	41	–	45	14	<10	<10	<10	12	11	<10	<10	<10	<10	<10	<10	<10
Cr	12	23	<10	9	<10	<10	9	61	28	<10	15	10	<10	<10	<10	21	<10	55	16	2	36	<10	<10	<10	12	17	17	<10	<10	<10	<10	<10
Cu	41	9	13	9	9	11	9	30	28	<10	<10	10	<10	7	8	21	2	2	2	14	<10	36	<10	83	11	18	17	15	<10	<10	<10	<10
Ni	24	50	<10	<10	<10	<10	11	35	<10	<10	8	<10	<10	7	8	13	14	15	13	<10	<10	17	10	35	35	24	18	17	20	17	15	9
Sc	23	15	11	4	<10	<10	5	24	27	5	8	13	10	7	8	13	14	15	13	11	8	17	10	35	35	24	18	17	20	17	15	9
Sr	190	200	160	70	70	85	69	180	110	164	60	100	100	90	54	100	74	220	138	100	70	80	60	380	200	480	240	330	150	150	100	87
V	220	120	<10	<10	<10	<10	<10	210	<10	<10	60	13	<10	11	8	25	45	52	45	21	70	80	60	64	7	<10	16	30	34	41	41	22
Zn	63	20	16	26	15	19	19	15	35	43	63	39	7	21	12	16	46	46	38	9	89	93	65	85	57	63	130	30	34	41	41	22
Zr	110	280	290	390	450	380	470	110	240	477	267	470	460	320	310	66	102	72	72	59	49	49	120	130	110	130	85	98	120	110	150	130
La	20	16	15	38	18	44	41	11	13	10	26	16	15	13	12	7	15	15	15	5	11	11	11	31	25	34	20	30	31	19	25	34
Ce	43	37	34	81	48	92	86	26	35	32	47	39	40	31	30	14	12	12	15	11	11	11	11	83	61	76	43	98	82	43	56	75
Pr	5.5	5.0	4.2	10	7	10	10	3.3	4.9	3.0	7.0	6.6	7.0	4.5	4.8	2.2	2.1	2.1	2.0	1.4	2.2	1.6	7.3	12	7.6	9.3	5.2	3.9	10	4.9	2.7	9.1
Nd	23	21	17	38	30	37	40	14	22	14	28	25	25	19	30	25	30	21	20	13	17	10	37	56	30	37	21	15	37	18	27	35
Sm	4.4	5.1	3.9	8.6	6.2	7.8	7.8	3.4	5.5	3.8	6.0	6.6	7.0	5.1	7.2	2.9	2.5	2.5	2.2	0.9	2.6	2.2	2.2	11	6.3	7.4	4.0	2.7	5.6	3.6	5.3	6.5
Eu	1.2	1.3	1.4	1.2	1.0	1.4	1.4	1.1	1.9	1.3	0.9	2.0	1.6	1.6	1.8	0.5	0.5	0.5	0.5	0.3	0.6	0.5	0.4	12	1.8	2.0	1.1	1.7	1.7	1.1	1.0	1.2
Gd	4.5	5.2	4.2	8.8	7.0	8.3	8.3	3.6	6.5	4.1	5.6	7.9	7.8	6.2	9.0	3.4	3.0	3.0	2.9	1.3	3.4	2.4	2.7	11.0	6.0	6.6	4.2	2.6	6.0	3.5	5.0	6.2
Tb	0.7	0.8	0.6	1.4	1.0	1.3	1.3	0.6	1.1	0.8	0.9	1.4	1.4	1.2	1.5	0.5	0.5	0.5	0.5	0.4	0.5	0.4	0.4	1.6	0.9	0.9	0.6	0.3	0.9	0.5	0.8	0.9
Dy	4.3	4.9	4.2	8.5	6.9	8.2	8.2	3.5	6.5	5.0	5.3	8.4	8.5	8.4	9.0	3.6	3.4	3.4	3.6	2.1	4.1	2.9	2.9	9.1	5.1	5.0	3.9	4.5	4.5	3.3	4.9	5.6
Ho	0.9	1.0	0.8	1.8	1.4	1.8	1.8	0.7	1.4	1.1	1.2	1.7	1.9	1.9	1.9	0.8	0.7	0.7	0.8	0.6	0.9	0.7	0.7	1.9	1.1	1.0	0.6	0.4	1.0	0.7	1.1	1.2
Er	2.8	2.8	2.5	5.1	4.2	5.0	5.0	1.9	4.2	3.1	3.3	5.4	5.4	6.0	5.8	2.4	2.2	2.2	2.4	1.8	2.9	1.9	2.0	5.3	3.0	3.0	2.4	1.2	2.9	2.2	3.3	3.5
Tm	0.37	0.45	0.36	0.84	0.64	0.81	0.81	0.27	0.64	0.53	0.57	0.78	0.84	0.91	0.87	0.35	0.34	0.34	0.37	0.27	0.43	0.31	0.31	0.80	0.48	0.48	0.42	0.20	0.44	0.37	0.56	0.62
Yb	2.6	2.9	2.5	5.3	4.4	5.4	5.4	1.9	4.8	3.8	4.3	5.8	5.9	6.6	6.3	2.4	2.1	2.1	2.5	2.0	3.1	2.3	2.1	5.3	3.3	3.5	2.9	1.5	3.1	2.5	3.9	4.2
Lu	0.4	0.5	0.4	0.9	0.7	0.81	0.81	0.27	0.66	0.62	0.72	0.86	0.88	0.93	0.88	0.35	0.34	0.34	0.36	0.29	0.47	0.32	0.31	0.8	0.5	0.5	0.3	0.3	0.5	0.4	0.7	0.7
Y	27	31	25	51	30	51	51	21	43	32	36	52	57	58	57	25	19	13	20	17	27	20	20	56	31	31	27	12	29	23	34	38
Ag	0.2	0.5	0.3	0.9	0.4	0.4	0.6	0.6	0.4	<0.2	<0.2	0.1	0.7	0.4	0.4	0.5	0.3	0.3	0.3	0.4	3.0	0.6	0.5	0.2	0.3	<0.1	0.2	<0.1	<0.1	0.2	0.4	0.4
Bi	<0.2	0.2	<0.2	<0.2	<0.2	0.2	0.2	0.1	1.0	<0.2	<0.2	0.9	11	0.7	1.2	0.5	0.3	–	–	<0.2	<0.2	<0.2	<0.2	<0.2	<0.2	<0.2	<0.2	<0.2	<0.2	<0.2	<0.2	<0.2
Cd	<0.2	<0.2	<0.2	<0.2	<0.2	<0.2	<0.2	<0.2	<0.2	<0.2	<0.2	<0.2	<0.2	<0.2	<0.2	0.5	–	<10	0.2	<0.2	<0.2	<0.2	<0.2	<0.2	<0.2	<0.2	<0.2	<0.2	<0.2	<0.2	<0.2	<0.2
Cs	0.70	0.51	0.22	0.54	0.43	0.67	1.30	0.19	0.83	0.24	0.25	0.21	0.21	0.10	0.05	0.20	0.07	0.07	0.03	0.24	0.14	0.12	0.46	0.42	0.09	0.29	0.29	0.28	0.24	0.52	0.52	0.11
Ga	22	18	18	18	17	16	17	21	21	20	17	18	16	17	19	12.0	12	13	13	10	13	9	10	19	20	19	15	15	16	14	13	16
Hf	3.0	6.2	6.0	9.2	9.1	8.7	10.0	3.5	5.5	9.8	6.8	9.5	9.1	6.7	7.0	2.20	2.98	2.20	2.43	1.8	1.4	1.4	2.8	2.1	2.7	2.8	2.1	2.3	2.8	2.7	3.9	3.1
In	0.07	0.07	<0.01	0.09	0.16	<0.01	<0.01	0.05	0.16	0.08	<0.2	0.05	0.07	0.05	0.1	<0.1	0.10	0.10	0.10	0.03	0.08	0.06	0.03	0.17	0.28	0.26	0.17	0.09	0.21	0.13	0.21	0.11
Mo	<0.1	0.3	0.10	0.8	0.60	0.10	0.8	4.8	0.8	0.3	<0.2	0.1	0.2	0.3	0.1	<0.1	1.1	1	1	0.3	0.5	1.7	0.3	0.5	0.8	0.6	1.9	0.5	0.9	2.9	0.8	0.8

Table 2 (Contd.)

Nb	10	18	16	11	23	22	12	10	9	11	13	10	16	3.5	3.3	14	3.6	2.2	1.9	1.9	3.4	10	6.7	12	7.2	6.2	9	10	12	11
Pb	1	3	2	1	4	4	1	4	4	1	2	2	3	3	2	2	2	1	10	6	12	2	2	15	5	3	9	2	6	2
Rb	28	6.4	5.1	14	23	30	4.0	25.0	10.0	14	2.7	9.7	2.3	8.7	16	6	11	11	8.4	10	6.9	13	4.3	8.4	19	11	19	17	11	18
Ta	0.4	0.5	0.8	1.1	1.4	0.9	0.5	0.6	0.6	0.4	0.8	0.5	0.9	0.2	1.2	0.90	1.4	0.58	0.1	0.1	0.2	0.7	0.9	0.8	0.5	0.6	0.5	0.8	0.7	0.6
Th	2.8	5.0	3.7	8.3	7.8	7.4	2.10	2.80	4.10	2.80	3.70	2.10	0.9	1.20	1.14		1.62	0.58	0.93	0.1	1.20	2.8	3.7	4.7	2.9	4.7	5.0	4.6	5.2	5.0
Tl	0.1	0.03	−0.0	−0.0	0.1	0.11	0.01	0.11	0.03	0.04	0.01	0.01	0.01	0.02	0.05	0.80	0.04	0.03	0.05	0.1	0.03	0.1	0.1	0.1	0.05	0.0	0.1	0.1	0.2	0.03
U	0.6	0.80	0.8	1.4	2.0	1.90	0.39	0.45	1.10	0.43	0.79	0.62	0.54	0.67	0.86	0.80	0.85	0.35	0.43	0.39	0.65	1.2	1.5	1.9	1.00	1.4	1.7	1.7	2.2	1.80
$(Th/Nb)_{NM}$	2.3	2.3	1.9	3.3	2.8	2.8	1.4	2.3	3.8	2.1	2.4	1.7	1.0	2.8	2.8	0.5	3.8	2.2	4.1	3.5	2.9	2.3	4.6	3.2	3.3	6.3	4.6	4.6	3.6	3.8
$(Th/La)_{NM}$	1.1	2.5	2.0	3.8	1.4	1.5	1.0	2.3	1.3	1.4	2.0	1.3	1.4	1.5	1.4	1.4	2.1	3.4	1.4	1.2	2.3	0.7	1.2	1.1	1.2	2.3	1.1	2.0	1.7	1.2
$(La/Yb)_{NM}$	5.2	3.80	4.1	2.80	8.1	5.2	3.9	1.8	4.1	1.9	1.7	1.3	1.3	1.9	1.9	2.0	1.7	0.5	1.2	1.6	1.4	4.0	5.2	6.6	4.7	7.7	8.3	5.2	4.4	5.5
$(Gd/Yb)_{NM}$	1.4	1.50	1.4	1.30	1.0	1.2	1.1	0.9	1.1	1.1	1.1	0.8	1.3	1.1	1.0	0.0	1.0	0.5	0.9	0.8	1.0	1.7	1.5	1.5	1.2	1.4	1.6	1.1	1.0	1.2
Y/Zr	1.7	3.7	4.8	3.9	5.2	3.8	2.3	14.9	7.4	3.7	3.3	2.3	2.2	1.1	2.2	1.4	1.5	1.4	0.7	1.0	2.5	0.6	1.5	1.7	1.3	3.3	1.7	2.0	1.8	1.4

tholeiite/calc-alkaline rocks. The exception is the quartz-diorite profile which has lower normalized REE concentrations as well as a steeper $(Gd/Yb)_N$ trend, suggesting a deeper, separate source from the more felsic phases in which amphibole, and possibly garnet, were stable. The BBIC and RLIC both have elevated light-rare-earth element (LREE) concentrations, and increasing $(TH/Nb)_N$ and $(La/Nb)_N$ ratios typical of more evolved, arc-related granitoids. The FPIC and BBIC show a decoupling between niobium and zirconium typical of relatively reduced melts, whereas the RLIC shows a more sympathetic Nb/Zr decrease relative to primitive mantle. This would suggest a more evolved, oxidized source.

The origin of all four composite intrusions as arc granitoids is supported by the Rb versus (Y + Nb) plot of the intrusions, which places them within the volcanic arc granitoid field (Pearce et al. 1984; Fig. 7A). All the suites have $(Gd/Yb)_N$ ratios of approximately one, typical of magmas derived from low-pressure, amphibole- and garnet-free source regions. This is supported by their low Al_2O_3 versus SiO_2 values indicating low-pressure, plagioclase-rich source areas (Barker and Arth 1976; Fig. 5E). The dominance of either plagioclase crystal fractionation or a plagioclase-rich restite is further supported by the La/Nb ratios for the four composite intrusions (Fig. 7B). If various average basalt compositions are considered as possible sources, the SLIC and FPIC could have been derived from primitive mantle, NMORB or arc tholeiite sources. The BBIC and RLIC are more likely related to a back-arc basalt precursor.

The development of all four composite intrusions in oceanic-arc tectonic regimes is supported by previous petrogenetic studies of their host volcanic successions. Stern et al. (1995) conclude that the host, bimodal volcanic rock succession to the SLIC was developed in a nascent oceanic-arc environment, whereas Barrie et al. (1993) postulate the initial rifting of a tholeiitic oceanic arc as the tectonic environment for the Noranda cauldron. Bailes and Galley (1996) postulate an evolved oceanic-arc regime for the fractionated volcanic succession which hosts the RLIC, whereas Sanborne-Barrie et al. (2001) suggest an evolved, continental marginal arc for the South Sturgeon cauldron which hosts the BBIC. The grouping of the SLIC and FPIC into primitive arc regimes, and that of the RLIC and BBIC into more evolved arc regimes is further supported by the composition of their associated VMS deposits. The deposits in the lower volcanic cycle in Snow Lake and in the Noranda cauldron are Zn-Cu-, Cu-Zn-, Cu-Zn-Au- and Cu-Au-rich, typical of high-temperature (350–450 °C) hydrothermal systems developed within primitive arc and rifted-arc, mafic, rock-dominated, bimodal volcanic successions. The VMS deposits within the middle volcanic cycle of Snow Lake and the Sturgeon Lake cauldron are Zn-Pb-Cu-Ag-rich and typical of evolved arc and back-arc, felsic, volcaniclastic rock-dominated successions.
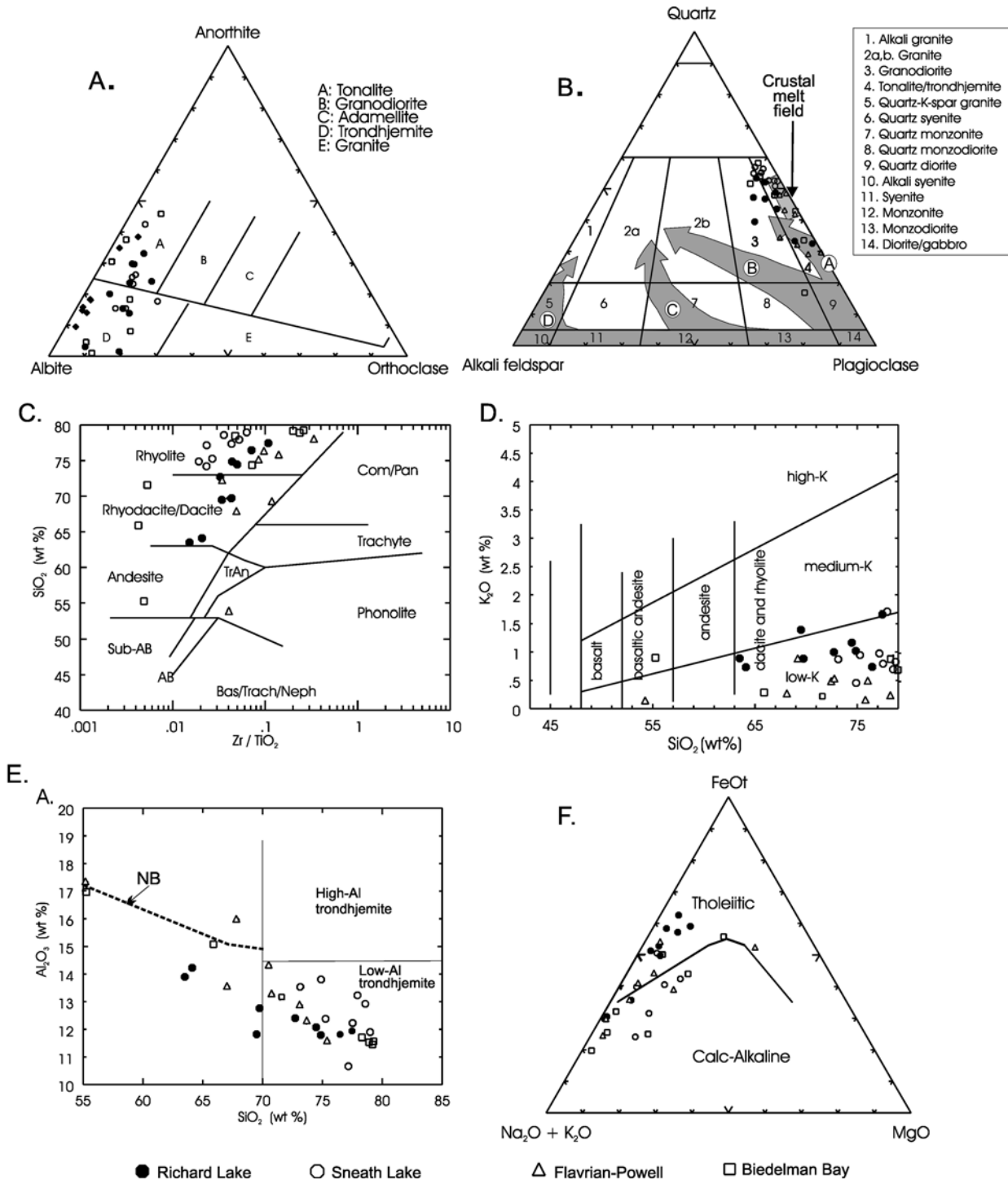
Fig. 5 A Normative feldspar ternary plot from O'Connor (1965) indicating that samples from all four intrusions fall within the tonalite and trondhjemite fields. **B** Normative alkali feldspar–quartz–plagioclase ternary plot from Lameyre and Bowden (1982) with fractionation trends from Lameyre (1987), demonstrating that some of the quartz diorite and tonalite from the four composite intrusions lie along the tholeiitic fractionation trend, whereas the trondhjemite samples are clustered about the field for tholeiitic crustal melts. **C** SiO_2 versus Zr/TiO_2 plot (Winchester and Floyd 1975) showing the distribution of intrusion samples from andesite (quartz diorite) to high-silica rhyolite (trondhjemite) fields, with the large majority of samples being trondhjemite to high-silica trondhjemite. **D** K_2O versus SiO_2 plot (Le Maitre 1989) showing a clustering of least-altered intrusion samples in the low-K field,

with the RLIC showing the most-evolved compositions. **E** Al_2O_3 versus SiO_2 plot indicating that samples with $SiO_2 > 70\%$ lie within the I-type, low-alumina trondhjemite field as defined by Barker (1979). Some of the tonalite and quartz-diorite samples lie along the New Britain (NB) trend for M-type oceanic-arc granitoids as defined by Whalen (1985). This indicates there may be both mantle and crustal melt sources for these Precambrian composite intrusions. **F** Normative alkali-total iron-magnesium ternary plot (Irvine and Baragar 1971) demonstrating that three of the four intrusions have tholeiitic compositions whereas the SLIC displays a more calc-alkalic character. This may be due to the extensive Mg-metasomatism which has affected both the volcanic and subvolcanic rocks in the Snow Lake VMS camp
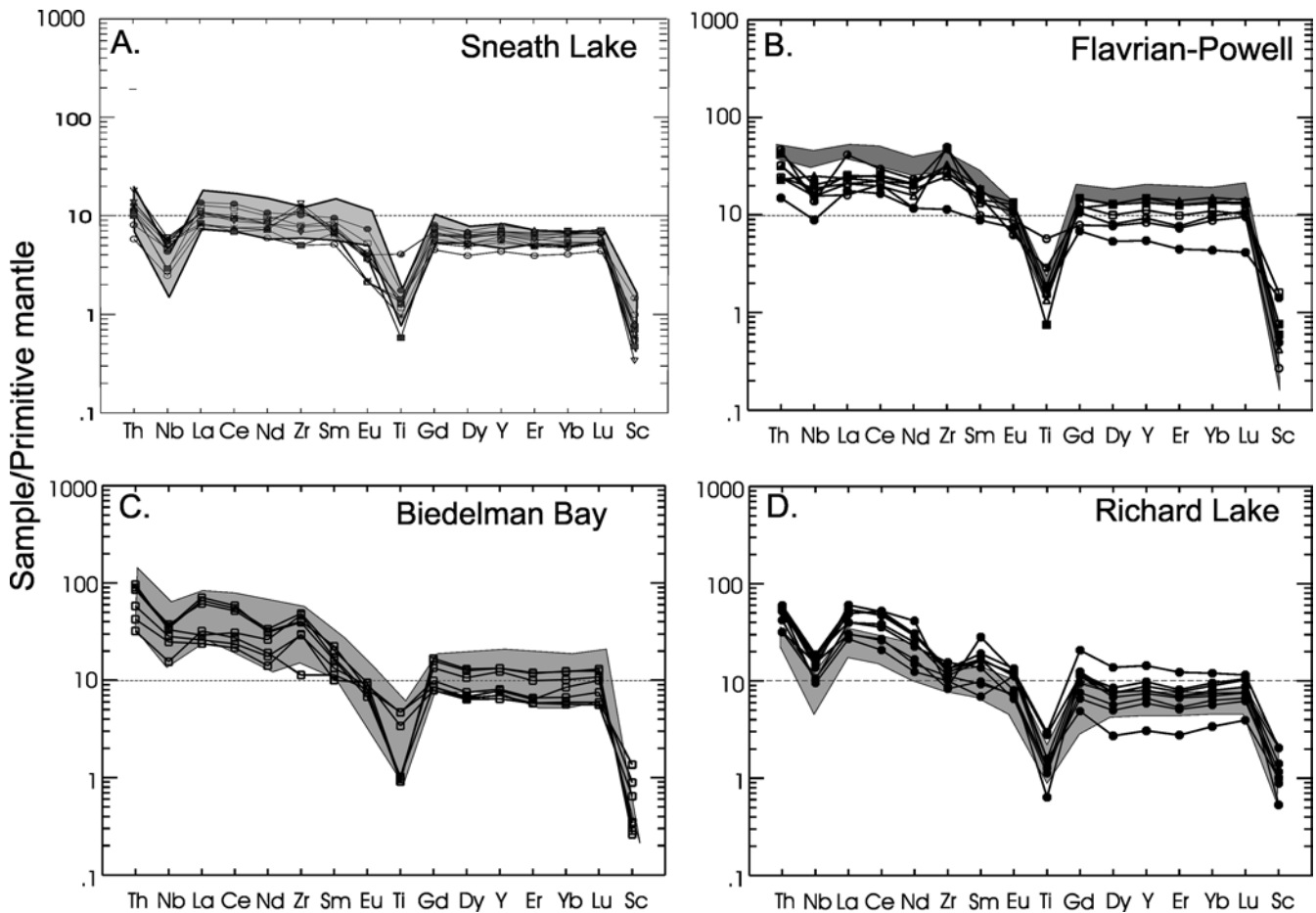
Fig. 6 Series of "spidergram" plots of REE and HFSE elements (plus Th) normalized to primitive mantle (Sun and McDonough 1989) for the **A** SLIC, **B** FPIC, **C** BBIC, and **D** RLIC. They are placed in order from most-primitive to most-evolved compositions. The large negative Nb anomaly for the SLIC does not indicate an evolved suprasubduction magma source but rather a strongly HFSE-depleted mantle typical of this Paleoproterozoic terrane. The shaded *areas* on each diagram represent the range of compositions for VMS-hosting rhyolites within the host volcanic successions. Rhyolite data for the Noranda area are from samples supplied by F. Santaguida, for Sturgeon Lake by J. Franklin, and for the Richard Lake area by S. Paradis

Alteration and mineralization

Mass-balance calculations

The calculation of net mass change and element redistribution during alteration of the various composite intrusions was carried out using the graphic isocon method of Grant (1986), modified by Huston (1993; Fig. 8; Table 3). This method was chosen because it allows for a graphic estimation of volume during alteration by measuring the change in the slope of a line defined by the altered/least-altered ratios for the most-immobile elements (Fig. 8). This is done in lieu of calculating volume through mass and density measurements. Sample density measurements were avoided due

to the density changes which both least-altered and altered rocks underwent during regional metamorphism. This is particularly true for phyllosilicate-rich altered rocks which have undergone amphibolite-grade metamorphism, resulting in drastic changes to both mineral type and grain size.

The method involves a comparison of selected element concentrations from altered samples with a least-altered precursor to determine the elements which were least mobile during the alteration process (Fig. 8). The concentration of least-mobile elements in least-altered rock versus altered rock is then used to determine the volume change undergone by the sample during alteration. This correction is added to a least-altered/altered ratio calculation to determine the degree of mobility undergone by other major and trace elements. Although the results were calculated as relative mass change in percent, they are presented here simply as element additions or subtractions in order to stress the importance of trends rather than quantitative change.

The four subvolcanic intrusive complexes are all altered to varying degrees. This is, in a large part, a result of their emplacement into a shallow, fluid-rich, subseafloor environment, although there is also abundant evidence for overprinting, synkinematic alteration and mineralization. The intimate association of the early

Fig. 7 A Rb versus (Y + Nb) plot (Pearce et al. 1984) showing the majority of the intrusion samples lying within the volcanic arc granitoid (*VAG*) field. None of the sample sets parallel fractionation trends for arc magmas, as defined by Christiansen and Keith (1996), suggesting that individual intrusions have more than one magma source. The extension of some sample groups into the within-plate granitoid field is a function of a high degree of fractionation. **B** Nb versus La plot (Thiéblemont et al. 1998) showing that, although most of the intrusion suites are dominated by either plagioclase fractionation or plagioclase-rich source areas, they appear to have different source compositions, as defined by average basalt ratios from different oceanic regimes. The SLIC shows the most primitive values, followed by the FPIC and BBIC. The scattering of RLIC values may indicate an influence of either spinel or amphibole in its restite
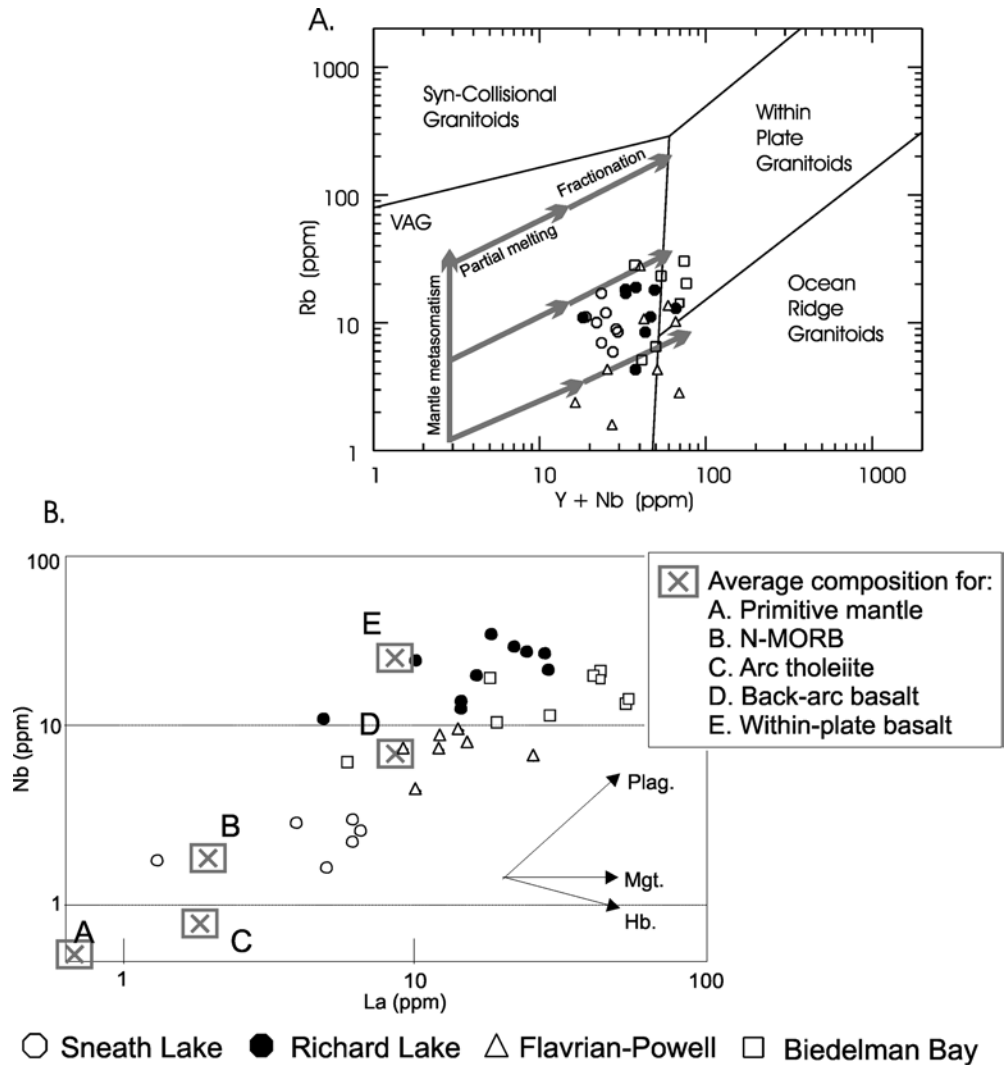
alteration zones with the cooling history of the subvolcanic intrusions can be confirmed in several ways. Some of the alteration zones have mineralogical and geochemical similarities with VMS-related alteration in the overlying volcanic strata. In many cases, altered intrusive phases are truncated by later unaltered, synvolcanic phases. The synvolcanic alteration zones have undergone the same degree of deformation as the host intrusions. Lastly, the alteration zones commonly have inherited an isotopic signature indicative of high-temperature seawater-rock reactions (Cathles 1993).

Intrusion-related alteration and mineralization can be divided into (1) hydrothermal-magmatic, (2) hydrothermal, (3) magmatic, and (4) synkinematic (Table 4). The hydrothermal-magmatic alteration is most commonly overprinted by hydrothermal alteration. Magmatic-related alteration usually forms a late-stage, dike-associated phase overprinting the subseafloor hydrothermal events. Synkinematic alteration and mineralization are associated with discrete fault and shear zones.

Hydrothermal-magmatic alteration

Although there is abundant evidence for the presence of metamorphic greenschist-grade mineral assemblages in the host volcanic rocks, this is usually restricted to fine-grained, disseminated replacement of the primary mineral assemblages (Hannington et al. 2002, this volume). Where seafloor hydrothermal alteration may be mistaken for greenschist-grade metamorphic effects, the former is readily identified by oxygen isotopic evidence (Kennedy 1985; Cathles 1993).

All four of the subvolcanic composite intrusions described here are affected to varying degrees by hydrothermal-magmatic alteration characterized by replacement and infilling by epidote, actinolite, quartz, albite, magnetite and subordinate sulfide minerals. Pervasive epidote–quartz replacement is most common within the early xenolithic phases. The tonalite or trondhjemite matrix to the more mafic xenoliths contains patches as much as several decimeters in diameter in which plagioclase has been replaced by epidote and
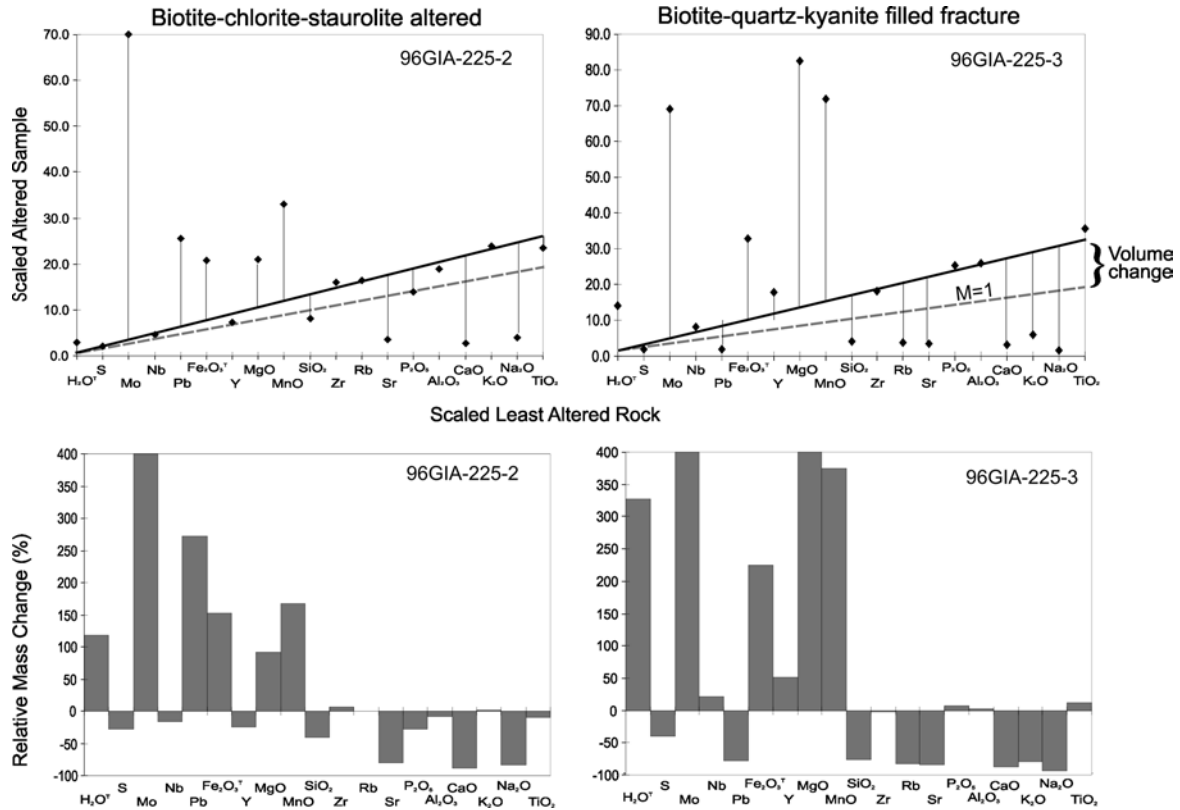
Fig. 8 An example of net mass-change calculations as devised by Grant (1986) and modified by Huston (1993) from two metamorphosed alteration facies affecting the east end of the SLIC below the Anderson and Stall VMS deposits. The *top* two diagrams compare least-altered trondhjemite versus altered trondhjemite for a number of elements commonly mobile in VMS hydrothermal systems. They are interspersed with a number of least-mobile elements which are used to define the baseline from which mass change is calculated, along with determining any volume change which took place during alteration. The *bottom* two diagrams are graphic representations of relative mass changes in percent

primary mafic minerals replaced with quartz, actinolite and magnetite. These patches can have centimeters-wide halos of silica-albite bleaching and/or dark actinolite-rich rims (Fig. 9A). In some cases, these epidosite replacement zones are fracture or vein controlled (Fig. 9B). In granophyre-rich intrusive phases, the quartz-albite spherulites are surrounded by actinolite-epidote-chlorite-rich mineral assemblages (Fig. 4D).

Alteration assemblages are also localized in miarolitic cavities, veins and vein breccias (Figs. 4A, B, and 9A–D). Miarolitic cavities in quartz diorite and tonalite are most commonly infilled with ferroactinolite, quartz and magnetite, and in trondhjemites with coarse-grained, euhedral to subhedral epidote, quartz ± magnetite. The pipe vesicles are infilled with epidosite and have strongly bleached and silicified margins (Fig. 4E). Straight-sided epidosite veins can have either bleached margins or dark, actinolitic margins (Fig. 9A). These can widen into epidosite-filled vein breccias which are decimeters wide (Fig. 9C). Other

veins are infilled with ferroactinolite–quartz–magnetite and ferroactinolite–magnetite–apatite ± pyrite ± chalcopyrite (Kennedy 1985; Fig. 9B). These vein types can also occur within the immediate wall rocks. Planar ferroactinolite veinlets, which are millimeters thick, also occur in the tonalite phases as widely spaced stockworks to centimeters-thick veins with epidote-rich altered margins (Fig. 9D). Where present in the same outcrop, epidote veins usually cut amphibole veins, although the presence of alteration halos of epidote surrounding some amphibole veins and amphibole on some epidote veins suggests that there may be a synchrony between the two end members.

Mass-balance calculations, based on the low mobility of titanium and zirconium, on the epidosite patches indicate cores enriched in calcium, strontium, lead and Fe^{+3}/Fe^{+2}, and depleted in copper, zinc, molybdenum, Fe^{+2}, magnesium, sodium, potassium and barium. The bleached margins to epidote-infilled miarolitic cavities are enriched in zinc, molybdenum, silica, sodium and CO_2, and depleted in silver, total iron, magnesium, calcium, strontium and barium. Epidosite vein bleached margins are depleted in total iron and magnesium (Table 4).

Hydrothermal alteration

Hydrothermal alteration is both fracture controlled and pervasive. The most common hydrothermal alteration is characterized by quartz–chlorite, quartz–chlorite–seri-

Table 3 Summary of the elemental changes which took place during various stages of alteration of the four synvolcanic composite intrusions

Type	Gains		Losses	
	Major	Minor	Major	Minor
Epidote veins				
Bleached margins (M = 0 to –10%) (M = –10 to –25%)[a]	Ca, Sr, Pb, CO_2	Zn, Ag, Fe^{+3}, Si	$Fe_{(t)}$, Mg	Ti
<u>Epidote cavity margins</u>				
Bleached margins (M = –10 to –25%) (M = –15 to –30%)	Zn, Mo, Si, Na, CO_2	Cu, S	Ag, $Fe_{(t)}$, Mg, Ca, Sr, Ba	
Epidosite patches	Ca, Sr, Pb, Fe^{+3}/Fe^{+2}	Si	Cu, Zn, Mo, Fe^{+2}, Mg, Na, K, Ba	
Amphibole alteration				
Fracture-controlled	$Fe_{(t)}$, Fe^{+2}, Mg, Ca, Cu, F		Al, Na, K, Ba	
Chlorite-altered fractures				
Weak (M < 5%)	H_2O, $Fe_{(t)}$, Cu, Pb, Mg, K, Ba		Ca, Na, Sr, Mo	
Moderate (M = 10–25%)	Cu, H_2O, Zn, Mo, Na, $Fe_{(t)}$, Fe^{+2}, Mg, K		Sr, Ca, Si	
Strong (M = 30–60%)	Cu, Zn, H_2O, Mo, $Fe_{(t)}$, Fe^{+2}, Mg		Ca, Na, Sr, CO_2, Ba	
Biotite alteration/veining				
Fracture-controlled margins (M = 0–10%)	Pb, Zn, Ba	K, Mg, Na	$Fe_{(t)}$, Mo, Ca, Sr, Ti, Si, Cu	

[a]M, Calculated volume change

cite or chlorite–sulfide mineral assemblages or their metamorphic equivalents (Fig. 10A, B). In the FPIC and BBIC, this alteration type can be confused with the regional greenschist-grade metamorphic overprint. The main differences are that what is defined as early hydrothermal alteration is either fracture controlled or pervasive within a discrete part of an intrusive phase. This contrasts with metamorphic mineral assemblages which will either be concentrated within synkinematic shears or homogeneously affect the entire intrusion. The fracture pattern which controls the chlorite and sericite-rich alteration within parts of the BBIC is clearly overprinted by the regional schistosity. Where the fractures are at an acute angle, the schistosity of the alteration assemblage is sheared. Where the schistosity is at a high angle to the fractures, there is a clear cross-cutting relationship (Fig. 10A). Field evidence for the pre-kinematic formation of alteration along fracture sets includes their truncation on a small scale by dikes related to overlying volcanic formations (Fee 1997) and by larger, late-phase resurgent stocks which are geochemically similar to earlier altered intrusive phases but appear to postdate VMS hydrothermal activity (Kennedy 1985; Bailes and Galley 1999).

The hydrothermal alteration assemblages form vein infillings and/or are part of a secondary alteration halo surrounding thin veins and fractures. Vein and fracture morphology can vary from columnar joints (Fig. 4H) through rectilinear (Fig. 10A) and anastomosing stockworks (Fig. 10B) to widely spaced, planar, parallel vein sets. The fracture sets are best developed and most intense along the margins of an intrusive complex, particularly within tonalite or trondhjemite phases.

The presence of chalcopyrite in the altered parts of the SLIC led Walford and Franklin (1982) to speculate on the presence of porphyry-like mineralization being associated with the VMS-forming process. Detailed mapping and core logging have resulted in the tracing of the Stall and Anderson VMS deposit foot-wall alteration/vein pipes down to the contacts with the SLIC (Bailes and Galley 1999; Fig. 10A–D). The VMS-related alteration appears to continue down into the subvolcanic intrusive complex. Both the volcanic and intrusive rocks have identical metamorphosed alteration mineral assemblages and display similar net mass changes. At near-constant titanium and zirconium, these changes include increases in water, total iron, magnesium, ferric iron, copper and zinc, with minor increases in potassium and barium relative to least-altered trondhjemite. The altered rocks may also be depleted in calcium, sodium and strontium, and more rarely silica and barium (Table 3). The reason for the identical alteration types in both the SLIC and overlying volcanic rocks is postulated to be collapse of a convective, subseafloor convection system into the cooling, composite intrusion. Further evidence that the alteration in both the volcanic rocks and intrusion is related to seawater-derived hydrothermal convection is given by the shift in whole-rock $\delta^{18}O$ to values of $< 6\%_{oo}$ (Cathles 1993; Fig. 11).

The BBIC associated with the Sturgeon Lake VMS camp shows evidence of pervasive alteration associated with the collapse of a subseafloor hydrothermal system. In this case, much of the composite intrusion is affected

Table 4 Summary of alteration and mineralization features within the four VMS-related composite intrusions

	Mineral assemblages	Alteration features	Setting	Type intrusion	Paragenesis
Hydrothermal	Quartz–chlorite–sulfide[a] Quartz–chlorite–sericite[a] Quartz–chlorite–biotite–garnet–magnetite[b] Quartz–chlorite–biotite–aluminosilicate[b]	Vein infilling and alteration halos on veins and fractures. Columnar joints, orthogonal fractures, anastomosing veins, planar vein/fractures	Commonly along intrusion margins and below VMS alteration pipes	Richard Lake, Sneath Lake, Flavrian-Powell, Beidelman Bay	Cuts magmatic-hydrothermal alteration
Magmatic-hydrothermal	Epidote–quartz Epidote–quartz–albite Epidote–quartz–magnetite Epidosite with quartz-rich margin Epidosite with actinolite-rich margin Actinolite–magnetite Actinolite–magnetite–apatite±pyrite, chalcopyrite Actinolite–magnetite with epidote-rich margin	Miarolitic cavities, pipe vesicles, veins, breccia veins, granophyre ground mass	Xenolith-rich tonalite and trondhjemite, quartz diorite, near volcano-intrusion and intrusion-intrusion contacts	Flavrian-Powell, Richard Lake, Sneath Lake	Earliest alteration type
Magmatic	Biotite veins and disseminations Extensive silicification Magnetite veins and breccia with sericite-rich margins Chalcopyrite, quartz–molybdenum, molybdenum veins and disseminations	Disseminations, veins and breccia veins	Centered on intrusive breccias and late porphyry dikes	Beidelman Bay, Flavrian-Powell	Commonly overprints the other two types
Synkinematic	Quartz–iron carbonate–chlorite–tourmaline (–sulfide)(–gold) Sericite–chlorite–carbonate Epidote–hematite	Shear-hosted veins and associated extensional veins Shear-hosted alteration and vein margins. Defines penetrative tectonic fabrics	Shears along intrusion margins, especially large, late mafic dikes. Also parallel to principal schistosity	Affects most synvolcanic intrusions	Overprints all synvolcanic features as late metamorphic event

[a]Mineral assemblage in greenschist-grade metamorphic terranes
[b]Mineral assemblage in amphibolite-grade metamorphic terranes
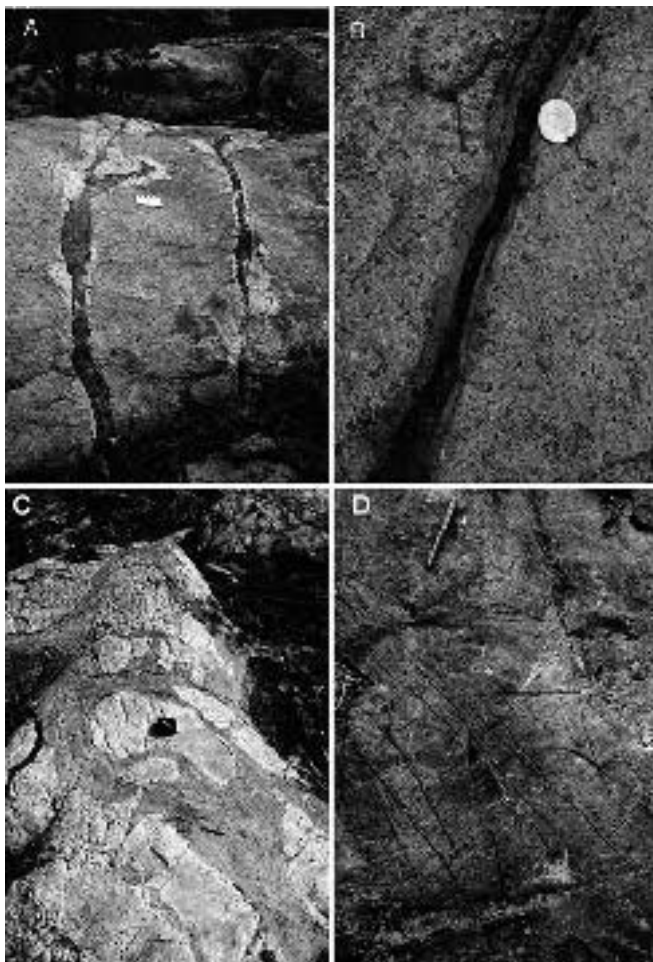
Fig. 9 A Epidosite veins with strongly silicified margins within the early trondhjemite phase of the FPIC (10-cm card for scale). **B** Ferroactinolite vein with strongly epidotized margins crossing the early trondhjemite phase of the FPIC. Note abundant amphibole-filled miarolitic cavities (4-cm coin for scale). **C** Epidosite-filled hydrothermal breccia hosted by a late trondhjemite phase within the core of the RLIC (6-cm camera lens cap for scale). **D** Thin (< 1 cm) amphibolite stockwork veins crossing the tonalite phase of the FPIC (12-cm pencil magnet for scale)

by a pervasive, low-grade carbonate alteration similar to much of the overlying volcaniclastic strata (Hudak 1996). More than 50% of the samples taken from the BBIC contain > 0.6% CO_2 and are thus strongly altered. Most of the carbonate is calcite or siderite, as confirmed by XRD analysis (Holk et al., unpublished data). Carbonate alteration associated with synkinematic fluid flow is commonly an Fe-dolomite and has an intensity controlled by discrete faults or shears. This does not appear to be the case for the carbonate alteration affecting much of the BBIC.

Magmatic alteration and mineralization

Magmatic-related alteration includes vein types and alteration facies most commonly cited as having been generated by the exsolution and migration of magmatic fluids during late-stage fractionation and crystallization of a magma chamber. In three of the four composite intrusions, distinctive alteration facies are spatially related to weak Cu–Mo mineralization. The presence of intrusion-hosted sulfide mineralization led researchers to suggest the intrusions supplied metals to the overlying, convective VMS-related hydrothermal systems (Poulsen and Franklin 1981; Walford and Franklin 1982; Kennedy 1985). The two best examples of this relationship occur within the FPIC and BBIC.

Along the western margin of the FPIC, a small trondhjemitic stock and associated porphyritic dike swarm are associated with the 600-m-diameter St. Jude intrusive-hydrothermal breccia pipe complex (Kennedy 1985; Carriere 1992; Fig. 2B). Copper–Mo mineralization in the pipe has a biotite alteration halo which, in turn, is surrounded by a sericite- and biotite-rich halo which hosts a number of polymetallic vein occurrences. The Powell segment of the FPIC contains the 44,000-t, Don Rouyn low-grade Cu–Mo(–Au) porphyry occurrence which is characterized by a bornite- and pyrite-rich core and a chalcopyrite- and pyrite-rich margin (Goldie et al. 1979; Jébrak et al. 1997). Associated alteration includes a silicic core, a biotite-rich margin and a halo of pervasively chlorite-altered tonalite and trondhjemite. The occurrence is spatially associated with abundant felsic and mafic dike swarms, but these show no documented temporal or genetic association with the mineralization.

The BBIC contains several subeconomic Cu–Mo occurrences (Friske 1974; Trowell 1974; Poulsen and Franklin 1981). These are associated with a series of intrusive-hydrothermal breccia pipes and a plagioclase–quartz porphyry dike swarm (Galley et al. 2000; Fig. 10C). The dike swarm and breccia pipes are the focus of several, apparently magmatic, alteration facies. This includes a broad zone of pervasive sericite–chlorite alteration which defines a crude halo about the porphyry dike swarm. It is characterized by elevated copper, zinc, molybdenum and fluorine concentrations (Galley et al. 2000). A series of magnetite veins and vein breccias with strongly sericite-altered margins occurs within the sericite and chlorite alteration zone (Fig. 10D). The zones of chalcopyrite–pyrite–pyrrhotite disseminations and veins have halos of secondary biotite with a red–orange birefringence and as much as 600 ppm Cu (Poulsen and Franklin 1981). The cores of these zones include strongly silicified trondhjemite which hosts planar quartz–molybdenum veins and veinlets.

The cogenetic relationship between porphyry type, intrusion-hosted sulfide mineralization and VMS mineralization in the host volcanic rock successions is brought into question by the U–Pb zircon dating of the intramineral dikes in the BBIC. Galley et al. (2000) demonstrated that these dikes are 14 Ma younger than the host tonalite–trondhjemite phases. This age difference is supported by the strongly calc-alkalic geochemical signatures of the dikes in comparison to the more
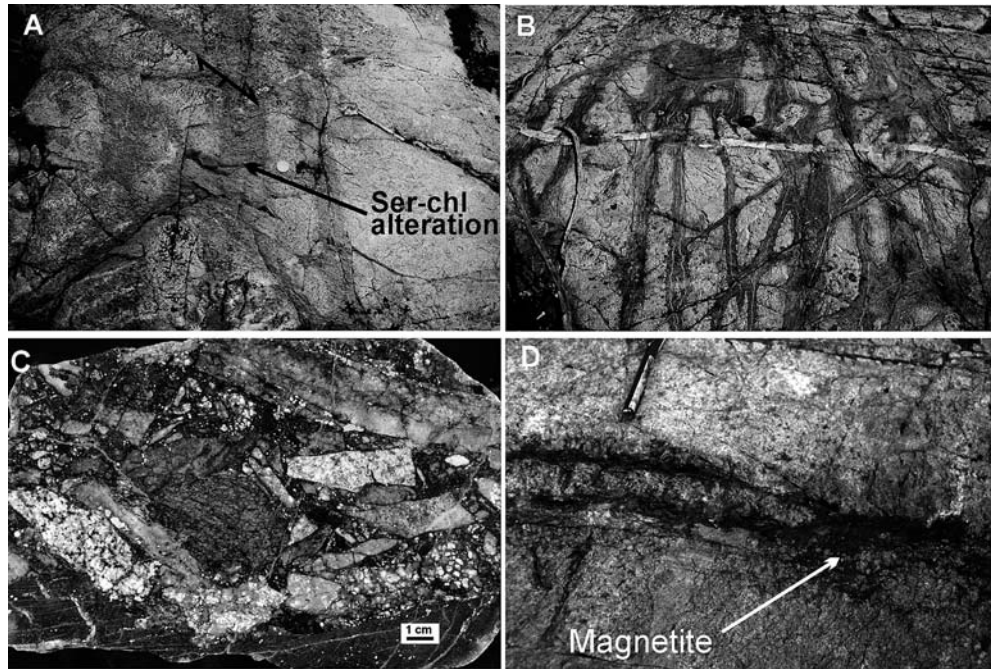
Fig. 10 A Chlorite-sericite-altered fracture system near the upper contact of the BBIC south of Beidelman Bay. The fracture system clearly predates the regional foliation which crosses at a high angle. Fractures subparallel to the foliation are strongly sheared (4-cm coin for scale). **B** Similar fracture system to that in **A** but metamorphosed to lower amphibolite grade to generate a distinctive quartz–biotite–chlorite–staurolite–kyanite assemblage. This latter fracture set transects the western margin of an early trondhjemite phase of the RLIC and is a product of Mg–Fe metasomatism (6-cm camera lens cap for scale). **C** Polished slab from an intrusive-hydrothermal breccia pipe associated with a 2,714-Ma porphyry dike swarm within the 2,734-Ma BBIC. The breccia pipe and dikes are the focus of Cu-Mo-rich quartz stockworks and sulfide disseminations. The fragment-supported breccia contains a variety of quartz-feldspar porphyry along with carbonate-altered mafic xenoliths. **D** An example of the magnetite veins and vein stockworks along the periphery of the quartz-feldspar porphyry dike swarm which host the Cu–Mo mineralization within the BBIC. Their strongly sericite-altered margins suggests their formation from a potassic fluid which released iron through biotite alteration of primary amphibole (end of pencil magnet for scale)

primitive geochemistry of the older phases of the composite intrusion.

Synkinematic alteration and mineralization

It is not unusual for synvolcanic intrusions to host synkinematic, shear-zone-hosted gold deposits, as there is commonly a large competency contrast between the intrusive-volcanic rock contacts. All four composite intrusions have been affected by at least two phases of deformation and accompanying metamorphism. Shear and fault zones commonly transect the intrusions, and these typically contain several generations of quartz- and carbonate-rich veins, some of which are auriferous. The BBIC contains extensive quartz–carbonate–chlorite ± tourmaline–sulfide veins, some of which were mined for

gold at the Darkwater Au deposit (Poulsen and Franklin 1981; Fig. 2A). Five gold deposits are hosted by the FPIC (Fig. 2B). These are controlled mainly by shear zones developed along Late Archean mafic dikes which strike NNW across the composite intrusion. There is no significant gold mineralization associated with either the SLIC or RLIC.

Synkinematic alteration commonly consists of iron carbonate–sericite–chlorite ± tourmaline-rich mineral assemblages along discrete shear zones. This is particularly the case with synvolcanic intrusions where the dominantly quartz- and plagioclase-rich primary mineral assemblages create very competent rocks in which the brittle-ductile shear zones commonly have sharp borders and restricted alteration halos.

Discussion

The importance of size, morphology and texture

Size, morphology and texture of igneous rocks are all useful field indicators for identifying shallowly emplaced, synvolcanic composite intrusions. The intrusions examined during this study have a limited area, as measured empirically by their strike length × dip-corrected thickness (Fig. 12). Calculation of volume is more difficult due to the variation in three-dimensional morphology displayed by high-level intrusions (Johnson and Pollard 1973; Roman-Berdiel et al. 1995). This has been attempted by treating the BBIC, FPIC and SLIC as circular sills, and the RLIC as a combination of circular sill and column (Fig. 12).

The calculated areas for all known VMS-related composite intrusions range from 10 up to 200 km^2 (Table 1; Fig. 12). Within this range, the majority,
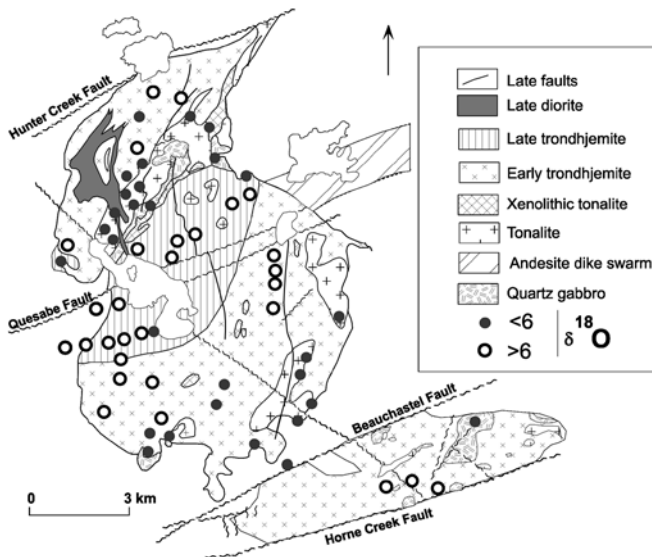
Fig. 11 Distribution of whole-rock $\delta^{18}O$ values from Kennedy (1985) and Cathles (1993) for the FPIC. Note that the late trondhjemite in the core of the composite intrusion shows little sign of high-temperature, seawater-derived hydrothermal alteration, whereas the early quartz-diorite and tonalite phases show the highest degree of alteration. The early-phase trondhjemite displays very erratic isotopic shifts, with the lowest $\delta^{18}O$ values in trondhjemite-hosting wall-rock pendants or xenoliths (geology from Kennedy 1985)

Fig. 12 The *top* diagram illustrates the relationship between the dip-corrected, calculated area for a number of VMS-related composite intrusions and the known aggregate tonnage for the associated VMS camps. Shallow dips for the FPIC, and both shallow dips and apparent thrust duplication for the Mule Mountain composite intrusion had to be taken into account. References for the physical dimensions of the intrusions defined by *open diamonds* are given in Table 1. The *bottom* diagram shows the calculated volume for each of the four intrusions described here versus total aggregate tonnage. The RLIC volume was crudely calculated as a combination of a column and a smaller disk, whereas an overall disk shape was assumed for the BBIC, FPIC and SLIC

including the four intrusions studied here, define a much smaller size range of 20 to 60 km^2. These calculated areas may, in some cases, be overestimated due to structural duplication, shallow dips and the presence of later magmatic phases. This includes the FPIC, whose shallow dips give a circular shape to what is actually a wedge-shaped sill (Bellefleur 1992).

When intrusion size is compared to the aggregate massive sulfide tonnage of the associated massive sulfide camp, there is a positive relationship with intrusions below 60 km^2 (Fig. 12). There is then a gap, with a group of larger synvolcanic intrusions whose size appears to be independent of the tonnage of the related massive sulfide camp. The exception may be the Murchinson-Darwin batholith which is associated with the massive sulfide-rich volcanic rocks of the Cambrian Mount Read (Large et al. 1996; Fig. 12). Intuitively, it is difficult to imagine how a batholith could be emplaced within a shallow subseafloor environment. Indeed, the restricted size range of most of the VMS-related subvolcanic intrusions, which includes the four described here, suggests that there are physical limitations on how large a subvolcanic intrusion may be. This problem has been studied by several authors in both the field and laboratory (Johnson and Pollard 1973; Corry 1988; Roman-Berdiel et al. 1995; Hogan et al. 1998), and is beyond the scope of the present paper. The complex internal stratigraphy of the studies' composite intrusions suggests variations in emplacement parameters during intrusion history. This includes variations in external stress fields, magma driving force, lithostatic pressure, and host-rock anisotropy as differences in both layer

competency and cross-stratal faults. The presence of post-VMS intrusive phases must also be taken into account when attempting to define what volume of magma was emplaced at what depth below the seafloor. It suffices to point out at this time that the empirical observation with respect to maximum size of VMS-related composite intrusions is one useful guideline for field identification of intrusions potentially involved in generating a subseafloor hydrothermal system.

The distribution of the internal phases is typically asymmetric for all four intrusions. Tonalite–trondhjemite stocks and dike swarms tend to occur below volcanic eruptive centers which occur along the intrusion strike length. In the cases of the SLIC and the RLIC, the greatest concentrations of stocks and dikes occur below felsic eruptive centers which host VMS deposits and occurrences (Bailes and Galley 1999; Fig. 2C). In the FPIC, dike concentrations and overall sill thickening are noted below both mafic and felsic rock, VMS-hosting eruptive centers (Gibson and Watkinson 1990; Richards 1999). These parts of each intrusive complex remain centers for magmatic activity during post-VMS volcan-

ism. In the case of the BBIC, this spans a time period of 14 Ma (Galley et al. 2000).

Finer-scale internal morphologies and textures are indicators of shallow (500–1,000 bar) emplacement of VMS-related intrusions. The ubiquitous presence of xenolith-rich phases is commonly evidence for the stoped emplacement of magmas initially as inclined dikes, which then evolve into sills within brittle crust (Johnson and Pollard 1973; Clemens and Mawer 1992; Leaman 1995). The formation of xenolithic phases is usually restricted to early stages of emplacement of the composite intrusions, which are commonly eclipsed by more massive trondhjemitic phases. The xenoliths rarely show signs of extensive assimilation, as the magmas are unable to transfer heat due to rapid cooling in a high-level subseafloor environment (Russell et al. 1995). Nevertheless, the presence of xenolithic phases appears to have a large impact on the volatile history of the composite intrusions. Isotopic and mineralogical evidence (Kennedy 1985) suggests that the included fragments of wall rock and early-stage, quartz-diorite and tonalite phases underwent extensive hydrothermal alteration prior to emplacement of late-stage trondhjemite phases. The presence of quartz–feldspar–amphibole pseudophenocrysts within xenoliths and pegmatitic overgrowths indicates that dehydration of the xenoliths has taken place (Castro et al. 1990). The abundance of miarolitic cavities infilled with hydrothermal minerals in the surrounding trondhjemitic host rocks is further evidence for excessive fluid accumulation in what are generally considered quite dry melts. This process can play an important role in volatile addition to the cooling magma (Russell et al. 1995; McLeod et al. 1998).

The presence of columnar jointing along the margins of both the FPIC and SLIC is further evidence for rapid cooling in a shallow crustal environment (Spry 1962). The alteration along the margins of these joint sets indicates that they played an important role in focusing hydrothermal fluid flow within the margins of these composite intrusions.

All four composite intrusions are characterized by large textural variations indicative of complex fractionation and cooling histories. Early quartz diorite and tonalite are fine-grained and commonly aphanitic to granophyric which suggests relatively rapid cooling, as would be expected in a shallow, fluid-rich, subseafloor environment. Trondhjemite phases vary from fine- to coarse-grained, and aphyric through seriate to quartz porphyritic. The coarse texture of the late-stage trondhjemite phases may be an indication of deeper emplacement depths. This would result not only in longer crystallization histories but also in changes in the ability of the magma to maintain volatiles during cooling (Hogan et al. 2000). The association of aplite and fine-grained porphyry dikes with the coarser-grained phases is also evidence that these late trondhjemites reached vapor saturation during late-stage crystallization. These textural changes from early to late stages of composite intrusion could reflect a thickening of the volcanic pile

during intrusion emplacement. This has implications with respect to the span of time over which the intrusions were emplaced relative to VMS hydrothermal activity.

Tectonic environment

The association of composite quartz diorite–tonalite–trondhjemite intrusions with clusters of VMS deposits is not an unexpected phenomenon in light of tectonic environments of these intrusions. The four intrusions studied all share the same, relatively primitive chemistry typical of granitoids emplaced within oceanic-arc regimes. This includes high Na/K, Fe^{+2}/Fe^{+3} and Zr/Ti ratios. Calcium and aluminum contents are low relative to the calc-alkalic tonalite–trondhjemite–granodiorite (TTG/TTD) suites typical of continental arc environments (Barker and Arth 1976; Drummond and Defant 1990). Low $(Gd/Yb)_{MN}$ and Al/Si ratios for the VMS-related intrusions are evidence for low-pressure source rocks lacking garnet and poor in subcalcic hornblende. Relatively low $(La/Sm)_{NM}$, $(La/Yb)_{NM}$ and Sr/Ti indicate very little input from an underlying, dehydrating subducting oceanic plate, as is typical for TTG magmatic suites, including adakites (Barnes et al. 1996; Beard 1998). These characteristics indicate that the four VMS-related composite intrusions were sourced from relatively low-pressure, immature suprasubduction environments.

These low-alumina synvolcanic composite intrusions are a product of low-pressure partial melting/fractionation processes within areas of oceanic-arc extension. The dominance of high-silica trondhjemites, with their high Zr/Ti ratios in each of these suites, suggests they formed as high-temperature (900–1,000 °C) partial crustal melts where temperatures were high enough to melt refractory minerals in which Zr commonly resides (Barrie et al. 1993; Barrie 1995). These felsic melts represent only a small volume (<10%) of the melt generated within dominantly basaltic regimes. The formation of the felsic melts is due to ponding of high-temperature (>1,400 °C) basaltic magma below a thinning mantle-crust interface, and the resultant low-pressure partial melting of small aliquots of the relatively anhydrous basalt–gabbro (Barker and Arth 1976; Huppert and Sparks 1988; Barnes et al. 1996). The difference in primitive-mantle-normalized REE profiles between the mafic and felsic components of the FPIC (Fig. 6B) is evidence for the involvement of two different magma sources, i.e., mantle and crust, in the formation of these composite intrusions. If this is the case, then these composite intrusions represent a transition between I- and M-type granitoids. This would further differentiate them from I-type TTG granitoids.

The generation of the felsic partial melts within a region of abnormally high heat flow would be ideal for the generation of a robust, subseafloor hydrothermal system (Barrie et al. 1999). These high-temperature,

low-viscosity melts would have the advantage of rising quickly up to a subseafloor environment where they could initiate and sustain large-scale, seawater convection systems. The abundance of dikes and stocks within and above the intrusions suggests a high degree of structural control during their emplacement history through synvolcanic faulting. These structures would focus both magma as feeder dikes and hydrothermal fluid upflow. This accounts for the strong spatial association between VMS deposits and rhyolites which are broadly comagmatic and coeval with the intrusions (Fig. 6A–D).

The differences between the primitive FPIC and SLIC composite intrusions and the relatively more evolved BBIC and RLIC intrusions are due to the types of extensional environments in which they formed. Stern et al. (1995) and Bailes and Galley (1996) define the lower volcanic cycle of the Snow Lake arc assemblage which hosts the SLIC as a nascent, arc extensional regime characterized by calcium-boninite and high-titanium basalt. The FPIC intruded the base of a cauldron formed by rifting of the Blake River tholeiitic arc (Peloquin et al. 1990; Barrie et al. 1993). In both cases, the host bimodal volcanic rocks are host to Cu–Au, Cu–Zn and Zn–Cu VMS deposits which are typical products of hot (350 °C) subseafloor hydrothermal systems (Gibson and Watkinson 1990; Bailes and Galley 1999). The RLIC and BBIC composite intrusions are associated with fractionated, volcaniclastic-dominated, VMS-hosting successions more typical of rift environments associated with more mature oceanic or continental margin arcs (Barrie and Hannington 1999). The VMS deposits above both of these intrusions are Zn-Pb-Cu-rich, and formed from lower-temperature (250–300 °C), more diffuse, hydrothermal fluid upflow (Morton et al. 1990; Bailes and Galley 1999). This association between VMS deposit type and composition of associated felsic rocks, which in turn is controlled in large part by the type of arc environment, has been explored by several researchers, including Lesher et al. (1985) and Barrie et al. (1993). Lesher et al. (1985) developed a system for classifying Archean VMS-related rhyolites by their chondrite-normalized La/Yb versus Yb ratios. This method can be used not only to identify low-alumina tonalite–trondhjemite suites which have the potential for being associated with VMS hydrothermal systems, but also to discern the type of VMS deposits which one would expect to be associated with them. The advantage of identifying a potentially composite intrusion, as opposed to a coeval rhyolite, is its possible relationship to a much larger, greenfields exploration target.

Emplacement timing relative to VMS formation

Observations on the evolution of each of the four studied composite intrusions with respect to their magmatic and hydrothermal history can be combined with known spatial relationships with the VMS host strata to determine their emplacement history relative to the VMS-forming hydrothermal events.

Beidelman Bay Intrusion

A large component of the BBIC of the Sturgeon Lake VMS camp appears to postdate the main VMS-forming hydrothermal events. Most of the biotite trondhjemite which comprises more than 75% of the composite intrusion shows little if any sign of pre-kinematic hydrothermal alteration. The exception is the western end of the trondhjemite, which is cut by pre-kinematic chlorite- and sericite-filled polygonal fractures which may be a product of VMS-related hydrothermal alteration. The upper contact of the unaltered biotite trondhjemite is in sharp contact with strongly silicified and garnet- and chlorite-altered basalts, suggesting intrusion into already hydrothermally altered strata. This is supported by the regional oxygen isotope survey completed by Holk et al. (unpublished data). The biotite trondhjemite has a similar composition and age to the Middle "L" rhyodacite pyroclastic flows which form the hanging wall to the F Group-Mattabi VMS deposits (Galley et al. 2000). This cumulative evidence indicates that a large part of the present BBIC was intruded after the F Group-Mattabi VMS event, with the biotite–trondhjemite perhaps representing a resurgent phase of late cauldron magmatism.

The presence of Co–Mo mineralization within the BBIC was in the past taken as evidence for a magmatically derived metal component added to the overlying VMS hydrothermal system. Galley et al. (2000) have demonstrated that the sulfide-mineralized porphyry dike swarm and intrusive-hydrothermal breccias are 14 Ma younger than the 2,734-Ma BBIC. The much more calc-alkalic nature of the mineralized porphyry dikes was an indication of the much more evolved compositions usually necessary for the development of magmatic Cu–Mo mineralization (Kelser et al. 1975; Lang and Titley 1998).

Flavrian-Powell Intrusion

There are several forms of evidence indicating the presence of intrusive phases within the FPIC which postdate the VMS-forming hydrothermal events of the Noranda cauldron (Fig. 13). A geological map of the Noranda area clearly demonstrates that the early trondhjemite phase of the FPIC intrudes the upper contact of the Amulet andesite, which is the immediate foot wall to the main VMS horizon. Although these contact relationships indicate that the early-stage trondhjemite represents a resurgent phase of late cauldron magmatism, it is overprinted by varying intensities of epidote alteration. Much of this epidote-rich alteration surrounds zones of xenolithic tonalite and early-stage trondhjemite in the form of epidote-quartz-filled miarolitic cavities, pipe vesicles and veins (Fig. 4B, C, F).
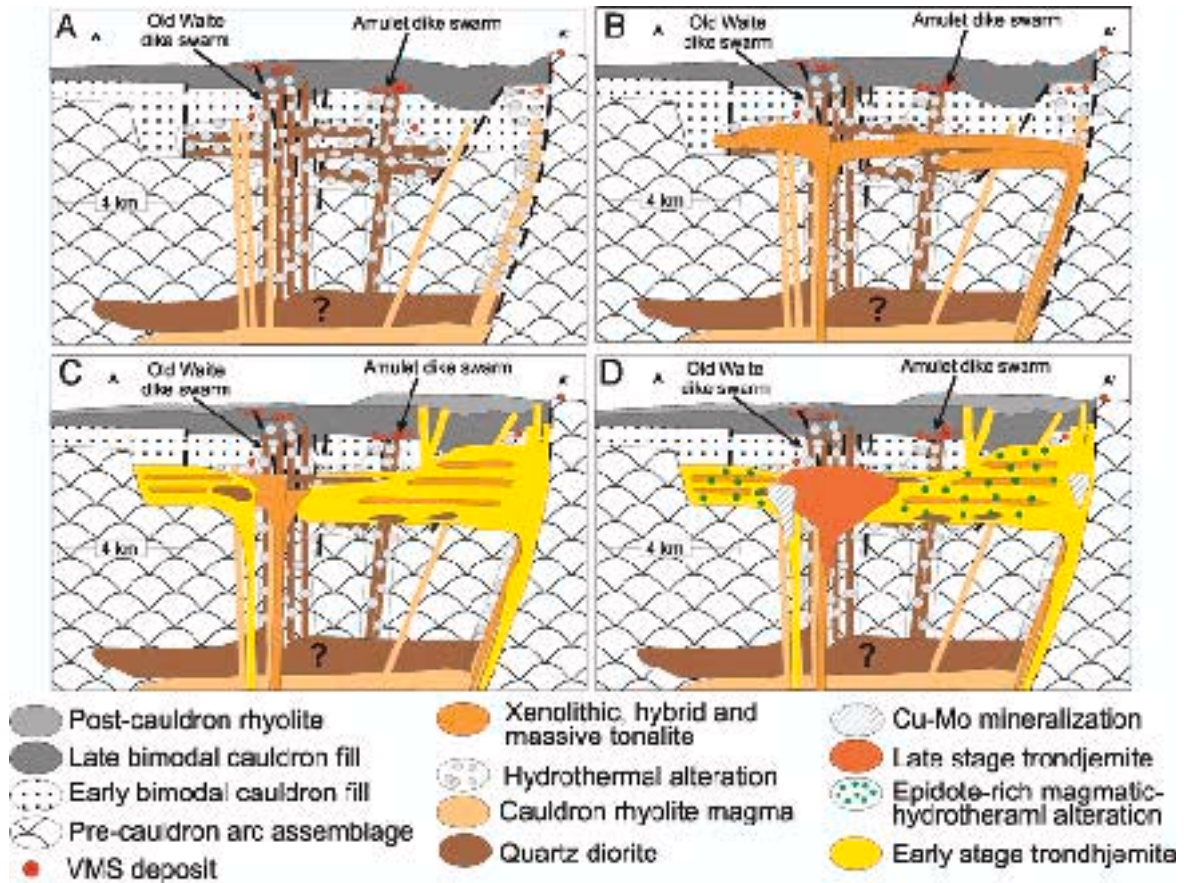
Fig. 13A–D The section A–A′ is shown on Fig. 2B bisecting the FPIC north to south. The FPIC emplacement history is as follows. **A** Hydrothermal activity related to the formation of the Noranda VMS deposits was instigated by high-level emplacement of the FLIC quartz-diorite sill-dike complex which fed andesitic flows within the overlying cauldron. The rhyolites within the cauldron were most likely fed from a hypothetical, deeper, felsic magma chamber. **B** During, or shortly after, the quartz diorite-related hydrothermal activity, a series of tonalite sills was emplaced at the same level as the quartz-diorite phase formed earlier. The forceful emplacement of the tonalite sills resulted in the brecciation and incorporation of the quartz-diorite phase and associated wall rocks. **C** Magmatism associated with late-stage cauldron formation resulted in the high-level emplacement of a number of trondhjemite bodies as sill complexes. The trondhjemite incorporated both the hydrothermally altered quartz-diorite and tonalite phases. The trondhjemite magmatism postdated the formation of the cauldron-hosted VMS deposits. **D** The partial assimilation of the hydrothermally altered quartz-diorite and tonalite phases caused the increased volatile content of the cooling trondhjemite which resulted in epidote-rich magmatic-hydrothermal alteration. The cessation of cauldron formation was followed by emplacement of a late trondhjemite phase and quartz-feldspar porphyry dike swarms. Associated with late-stage magmatism was the formation of Cu-Mo-rich intrusive-hydrothermal breccia pipes and a small porphyry system

The pendants and xenoliths of quartz diorite and basalt can have $\delta^{18}O$ values as low as 1.5‰, indicating intense, high-temperature (> 350 °C) interaction with a fluid derived from seawater (Kennedy 1985; Cathles 1993). Early-stage trondhjemite in contact with, or proximal to, wall-rock xenoliths and pendants has $\delta^{18}O$ values from 5 to 6‰. Away from the pendants of tonalite and xenolithic trondhjemite, the early-stage trondhjemite has a range of normal magmatic $\delta^{18}O$ values typical for a felsic granitoid (6 to 9‰; Fig. 11). The evidence for volatile exsolution in the early-stage trondhjemite, and the accompanying isotopic shift may be evidence that the hydrothermal alteration signature of the early trondhjemite was inherited through volatile release from previously altered, wall-rock xenoliths.

The xenoliths rarely show signs of assimilation, which indicates the inability of the magma to transfer heat, due to its rapid cooling in a high-level subseafloor environment (Russell et al. 1995). The host intrusion may form thin, centimeters-wide, pegmatitic rims surrounding the xenoliths, indicating volatile concentration during crystallization (Fig. 4C). Quartz diorite and mafic volcanic rock xenoliths commonly contain millimeter-sized ovoids of quartz, with feldspar and amphibole rims, which are postulated to be a product of metasomatism due to partial digestion (Castro et al. 1990). Both of these features may be textural evidence for "assimilation dehydration" during which fluids are extracted from previously altered, wall-rock xenoliths and added to the host magma. The abundance of miarolitic cavities in the xenolith zones indicates localized volatile oversaturation of the host, early-stage trondhjemite. This process can play an important role in volatile addition to the cooling magma (Russell et al. 1995; McLeod et al. 1998).

Sneath Lake Intrusion

The SLIC also shows evidence that at least part of its emplacement history took place after formation of the cycle-1 Cu–Zn VMS deposits (Fig. 14). Only the tonalite and trondhjemite stocks, clustered at either end of the composite intrusion, are hydrothermally altered to any extent. These stocks lie directly beneath and, in some cases, intrude the VMS-mineralized rhyolites which have been demonstrated to be comagmatic with the SLIC (Bailes and Galley 1999; Fig. 6A). The quartz megacrystic trondhjemite sill which forms the center of the SLIC is not only unaltered but contains chlorite-staurolite-garnet-rich xenoliths and pendants of previously altered trondhejmite. The quartz phyric trondhjemite stock at the eastern end of the SLIC clearly represents a post-VMS intrusive phase because it has enveloped the Rod VMS deposit. It appears then that only the quartz diorite(?)–tonalite–trondhjemite stocks directly below the VMS-hosting rhyolites were present at the time of VMS-related hydrothermal alteration.

Much of the SLIC may have been involved in hydrothermal activity which postdated VMS mineralization and took place at the end of cycle-1 volcanism. The top of cycle 1 is defined by the so-called Foot-Mud horizon, a meters-thick unit of sulfidic mudstone-chert and felsic epiclastic rocks (Bailes and Galley 1999). The strike length of this sulfidic unit is almost identical to that of the underlying SLIC. Furthermore, it is underlain along its entire strike length by several hundred meters of variably silicified basaltic andesite (Skirrow and Franklin 1994). The high $\delta^{18}O$ values for the silicified mafic volcanic rocks (Taylor and Holk 1998) suggest the alteration was a product of relatively low-temperature, subseafloor seawater-rock interaction. The entire SLIC may have, therefore, acted as a heat source to generate a shallow, diffuse but areally extensive, hydrothermal event which resulted in the hydrothermal component of the Foot-Mud horizon.

Richard Lake Intrusion

The spatial and cross-cutting relationships of the bulk of the RLIC with respect to hydrothermally altered wall rocks suggest that most of the composite intrusion was emplaced after VMS-related hydrothermal activity (Fig 15). There is almost a direct correlation between the location of the early emplaced dacite–tonalite sill-dike swarm and the intensity of hydrothermal alteration in the overlying volcanic strata (Skirrow and Franklin 1994; Bailes et al. 1996; Bailes and Galley 1999). The first phase of quartz phyric trondjemite which occupies much of the lower half of the RLIC is affected by fracture-controlled Fe–Mg metasomatism similar to that affecting the early dacite–tonalite sill-dike swarm (Fig. 10B). The remainder of the trondhjemite and aplite phases are unaffected by the chlorite- and
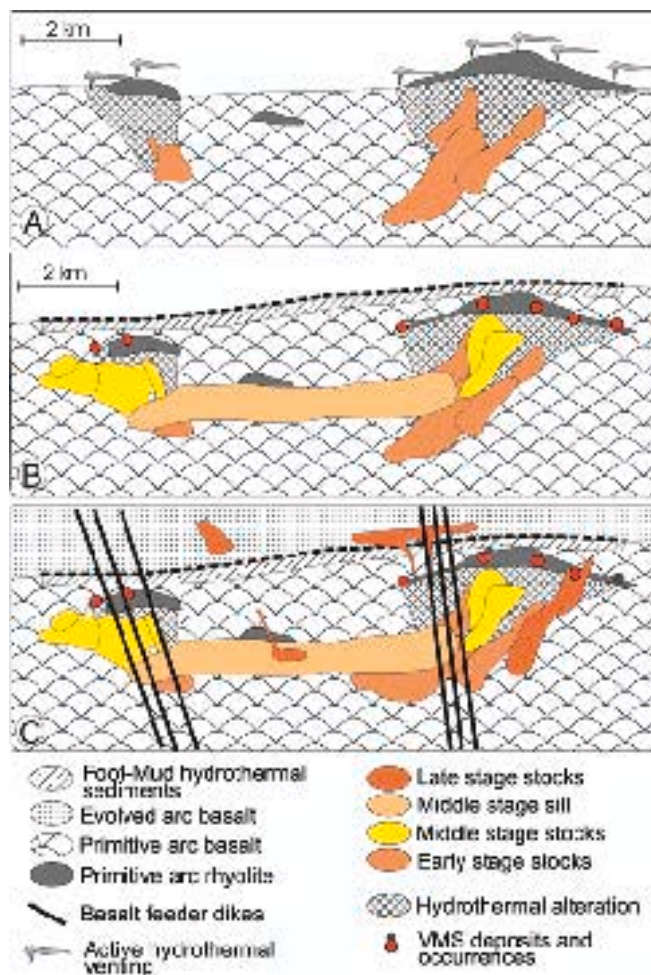
Fig. 14 A The formation of the SLIC in the Snow Lake primitive arc assemblage began with emplacement of tonalite and trondhjemite stocks below comagmatic rhyolite extrusive centers. Their emplacement initiated convective hydrothermal activity centered on the overlying rhyolite and resulted in the formation of VMS deposits. **B** Middle-stage felsic magmatism resulted in the further emplacement of stocks, possibly within the active hydrothermal system. Post-VMS intrusion of a large trondhjemite sill joined the separate intrusion complexes into one large sill complex. This sill appears to be responsible for renewed hydrothermal activity at the end of primitive arc volcanism, and the formation of an extensive exhalite horizon. **C** Late-stage stock and sill intrusion resulted in overprinting of the comagmatic rhyolite and envelopment of one of the VMS deposits. Mafic dike swarms associated with flows within the overlying, mature arc assemblage are focused on the earlier, primitive arc felsic magmatic centers, suggesting long-term control on magmatism by major synvolcanic structures

aluminosilicate-rich alteration. This suggests that the early quartz phyric trondhjemite intruded into, and perhaps terminated, the VMS hydrothermal system developed earlier, and that the later trondhjemite–aplite phases postdated it. The origin of the epidote-rich cavities, veins and hydrothermal breccias is unknown. The fact that this alteration overprints the core of the composite intrusion and that it increases in intensity towards the core suggests it is a late-stage crystallization phenomenon.
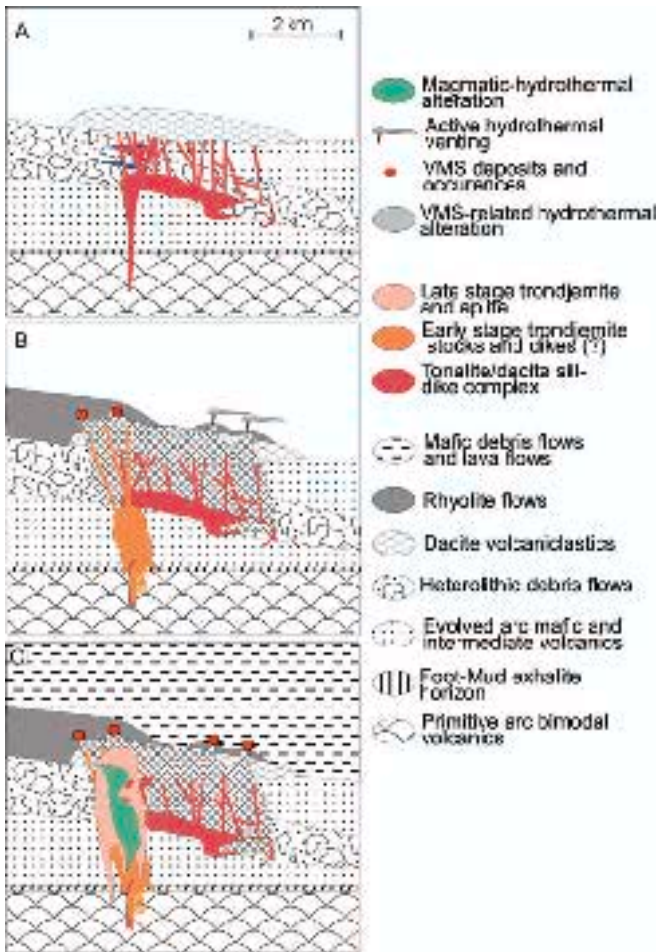
Fig. 15 A The RLIC evolved from an early sill-dike complex into a series of overprinting stocks and late dikes. The early tonalite–dacite sill-dike complex formed at the contact between underlying, pillowed basalt flows and overlying, mafic volcaniclastic units. The sill-dike complex acted as a shallow reservoir for a dacite volcanic formation approximately 2,000 m upsection. The sill-dike swarm was also the center for VMS-related hydrothermal activity which resulted in the formation of a series of Zn-Pb-Cu-rich massive sulfide deposits. **B** The next stage of intrusive activity involved emplacement of a tonalite stock. Hydrothermal alteration along the stock's margins indicates intrusion during the VMS-related hydrothermal event. **C** Early-stage magmatism was followed by post-hydrothermal emplacement of a number of trondhjemite stocks, and finally an aplite dike swarm. Associated with formation of the late-stage aplite dikes was epidote-quartz-rich magmatic-hydrothermal alteration centered on hydrothermal breccias, veins and miarolitic cavities

Conclusions

The study of four Precambrian synvolcanic composite intrusions has demonstrated that they have characteristics which make them high profile targets for VMS exploration. The fact that >80% of known, VMS-related subvolcanic intrusions are low-alumina quartz diorite–tonalite–trondhjemite in composition indicates that they form in unique tectonic environments, which is common to a large majority of Precambrian VMS deposits. These are extensional regimes within oceanic island arc envi-

ronments which may form as either nascent arc or primitive arc rifts. In both cases, crustal thinning and subsequent mantle decompression results in basalt magma underplating and subsequent high-temperature partial crustal melting. The result is the generation of bimodal volcanic environments in which persistent thermal corridors are maintained by the presence of a succession of high-level composite intrusions. Their high initial temperatures and anhydrous compositions allow them to rise rapidly to shallow crustal levels. This results in an efficient heat transfer from the magmas to the surrounding, fluid-rich volcanic pile and the initiation of convective hydrothermal fluid flow. Differences in crustal thickness, where rifting is initiated, most likely controls magma composition and the ratio of mafic (mantle) to felsic (crustal) volcanism which, in turn, has an impact on the type of VMS deposits to form. In more primitive, mafic volcanic rock-dominated extensional regimes, the composite intrusions have a tholeiitic composition and associated VMS deposits are Cu(-Au)-rich. The rifting of thicker arc crust, where partial crustal melting takes place at higher pressures, results in a more felsic-dominated, calc-alkalic character for the volcanic succession and the associated composite intrusions. The VMS deposits in these environments tend to be more Zn-Pb-Ag-rich.

The similarity in composition between VMS-related composite intrusions and VMS-hosting rhyolites makes the former optimum exploration targets due to their larger size. The apparent restriction in the size of most VMS-related composite intrusions to between 10 and 60 km^2 may well be a function of their shallow emplacement depths. The four intrusions studied are all within 2,000 m of VMS mineralization in the overlying volcanic strata, with some late-stage phases transecting the VMS-hosting strata. In the cases of the FPIC, SLIC and RLIC, significant VMS mineralization is restricted to above the strike length of the composite intrusions, as are related extensive exhalite formations. The asymmetric distribution of internal phases within the composite intrusions further restricts the most likely locations for VMS deposits in the host volcanic rock succession. Abundant stocks and dike swarms commonly underlie eruptive centers in which VMS deposits most typically form.

Subvolcanic composite intrusions are typified by wide variations in contact relationships, textures and grain size. In general, early quartz-diorite and tonalite phases occur as xenoliths in later trondhjemite phases or are cut by sharp-sided trondhjemite and aplite dikes. The trondhjemite phases are the most voluminous and contain variably sharp to gradational contacts indicating closely spaced pulses of compositionally similar magma. The early phases are commonly fine-grained and aphyric to granophyric, whereas the trondhjemite phases are fine- to coarse-grained equigranular, seriate to granophyric, with associated aplite and porphyry dikes. This temporal variation in grain size indicates a thickening of the volcanic rock pile during intrusion emplacement, implying that late-stage trondhjemite phases may post-date principal VMS activity in the camps.

The presence of both pre- and post-VMS phases to the composite intrusions is apparent in all four cases. Early quartz-diorite and tonalite phases are strongly affected by hydrothermal alteration zones spatially associated with VMS-related alteration within the host volcanic rock successions. Trondhjemite phases commonly transect the volcanic rock-hosted alteration zones and, in some cases, they intrude up through the principal VMS horizons. Trondhjemite and associated aplite and porphyry dikes are affected by mostly epidote-quartz-albite-rich alteration which is associated with late-stage volatile exsolution. In some cases, volatiles appear to have been added to the trondhjemite melts through dehydration of previously altered, wall-rock xenoliths. Dating and composition of the trondhjemite phases indicate that they are still broadly coeval with rhyolites within the volcanic host-rock successions, and can be considered part of resurgent magmatic activity slightly postdating the time of VMS mineralization. In the case of the Sturgeon Lake and Noranda VMS camps, these resurgent phases may be responsible for VMS mineralization higher in the volcanic rock pile. The bracketing of the age of VMS mineralization in the three Precambrian VMS camps by associated composite intrusions does not affect their usefulness as greenfields exploration targets, as they still assist in determining the presence of a thermal corridor within which there is the greatest potential for locating significant VMS mineralization. The presence of both pre- and post-VMS phases does raise a note of caution for researchers modeling these intrusions for heat-flow studies which are used to understand the formation of subseafloor hydrothermal systems.

References

Abraham APG, Davis DW, Kamo SL, Spooner ETC (1994) Geochronological constraints on late Archean magmatism, deformation and gold-quartz vein mineralization in the northwestern Anialik River greenstone belt and igneous complex, Slave Province, N.W.T. Can J Earth Sci 31:1365–1383

Alabaster T, Pearce J (1985) The interrelationship between magmatic and ore-forming hydrothermal processes in the Oman ophiolite. Econ Geol 80:1–16

Albers JP, Bain JH (1985) Regional setting and new information on some critical geological features of the West Shasta District, California. Econ Geol 80:2072–2092

Allard GO (1976) Dore Lake Complex and its importance to Chibougamau geology and metallogeny. Ministère Rich Nat Québec Rapp DP-368

Alldrick DJ (1978) Aeromagnetic analysis of the Copperton volcanic Belt, South Africa. MSc Thesis, Imperial College, London

Alt JC (1995) Sub-seafloor processes in mid-ocean ridge hydrothermal systems. In: Humphris SE, Zierenberg RA, Mullineaux LS, Thomson RE (eds) Seafloor hydrothermal systems: physical, chemical, biological, and geological interactions. Am Geophys Union Monogr 91:222–272

Ames DE, Bleeker W, Heather KB, Wodicka N (1997) Timmins to Sudbury transect: New insights into the regional geology and setting of mineral deposits. Geol Assoc Can Field Excur Guide B6, pp 38–71

Ashwal LW, Morrison DA, Phinney WC, Wooden JL (1983) Origin of Archean anorthosites: evidence from the Bad Vermilion complex. Contrib Mineral Petrol 82:259–273

Bailes AH, Galley AG (1996) Setting of Paleoproterozoic volcanic-hosted massive base metal sulfide deposits, Snow Lake. In: Bonham-Carter GF, Galley AG, Hall GEM (eds) EXTECH I: A multidisciplinary approach to massive sulfide research in the Rusty Lake-Snow Lake Greenstone Belts, Manitoba. Geol Surv Can Bull 4236:105–138

Bailes AH, Galley AG (1999) Evolution of the Paleoproterozoic Snow Lake arc assemblage and geodynamic setting for associated volcanic-hosted massive sulfide deposits, Flin Flon Belt, Manitoba. Can J Earth Sci 36:1789–1805

Bailes AH, Hunt PA, Gordon TM (1991) U-Pb zircon dating of possible synvolcanic plutons in the Flin Flon belt at Snow Lake, Manitoba. Geol Surv Can Radiogenic Isot Stud 4:35–43

Bailes AH, Galley AG, Skirrow RG, Young J (1996) Geology of the Chisel volcanic-hosted massive sulfide area, Snow Lake, Manitoba (part of 63 K/16SE) (1:5 000). Geol Surv Can Open File 3262

Barker F (1979) Trondhjemite: Definition, environment and hypothesis of origin. In: Barker F (ed) Trondhjemites, dacites, and related rocks. Elsevier, New York, pp 1–11

Barker F, Arth JG (1976) Generation of trondhjemitic-tonalitic liquids and Archean bimodal trondhjemite-basalt suites. Geology 4:596–600

Barnes CG, Peterson SW, Kistler RW, Murray R, Kays MA (1996) Source and tectonic implications of tonalite-trondhjemite magmatism in the Klamath Mountains. Contrib Mineral Petrol 123:40–60

Barrett TJ, MacLean WH (1999) Volcanic sequences, lithogeochemistry, and hydrothermal alteration in some bimodal volcanic-associated massive sulfide systems. Rev Econ Geol 8:101–133

Barrie CT (1995) Zircon thermometry of high-temperature rhyolites near volcanic-associated sulfide deposits. Geology 23:169–172

Barrie CT, Davis DW (1990) Timing of magmatism and deformation in the Kamiskotia-Kidd Creek area, western Abitibi Subprovince, Canada. Precambrian Res 46:217–240

Barrie CT, Krogh TE (1996) U-Pb zircon geochronology of the Selbaie Cu-Zn-Ag-Au Mine, Abitibi Subprovince, Canada. Econ Geol 91:563–575

Barrie CT, Hannington MD (1999) Introduction: Classification of VMS deposits based on host rock composition. Econ Geol Monogr 8:2–10

Barrie CT, Ludden JN, Green AH (1993) Geochemistry of volcanic rocks associated with Cu-Zn and Ni- Cu deposits in the Abitibi Subprovince. Econ Geol 88:1341–1358

Barrie CT, Cathles LM, Erendi A (1999) Finite element heat and fluid flow computer simulations of a deep ultramafic sill model for the giant Kidd Creek volcanic-associated massive sulfide deposit, Abitibi Subprovince, Canada. Econ Geol Monogr 10:529–540

Beard JS (1998) Polygenetic tonalite-trondhjemite-granodiorite (TTG) magmatism in the Smartville Complex, Northern California, with a note on LILE depletion in plagiogranites. Mineral Petrol 64:15–45

Bellefleur G (1992) Contribution des méthodes de potential à la structure profonde dans le Group de Blake River, Abitibi. MSc Thesis, Ecole Polytechnique, Montreal

Bergström U, Billström K, Sträng T (1998) Age of the Kristineberg Pluton, western Skellefte District, northern Sweden. Sver Geol Undersog 557:24–27

Brauhart CW, Groves DI, Morant P (1998) Regional alteration systems associated with volcanogenic massive sulfide mineralization at Panorama, Pilbara, Western Australia. Econ Geol 93:292–302

Calvert AJ (1995) Seismic evidence for a magma chamber beneath the slow spreading Mid-Atlantic Ridge. Nature 377:410–413

Campbell IH, Franklin JM, Gorton MP, Hart TR, Scott SD (1981) The role of subvolcanic sills in the generation of massive sulfide deposits. Econ Geol 76:2248–2253

Carriere A (1992) Le porphyre à Au-Mo de Saint-Jude. BSc Thesis, Université du Québec à Montreal

Castro A, de la Rosa JD, Stephens WE (1990) Magma mixing in the subvolcanic environment: petrology of the Gerena interaction zone near Seville, Spain. Contrib Mineral Petrol 105:9–26

Cathles LM (1977) An analysis of the cooling of intrusives by groundwater convection which includes boiling. Econ Geol 72:804–826

Cathles LM (1983) An analysis of the hydrothermal system responsible for massive sulfide deposition in the Hokuroko basin of Japan. Econ Geol Monogr 5:439–487

Cathles LM (1993) Oxygen isotope alteration in the Noranda mining district, Abitibi Greenstone Belt, Quebec. Econ Geol 88:1483–1511

Christiansen EH, Keith JD (1996) Trace element systematics in silicic magmas: A metallogenic perspective. In: Wyman DA (ed) Trace element geochemistry of volcanic rocks: applications for massive sulfide exploration. Geol Assoc Can Short Course 12:115–154

Clemens JD, Mawer CK (1992) Granitic magma transport by fracture propagation. Tectonophysics 204:339–360

Collier J, Sinha M (1990) Seismic images of a magma chamber beneath the Lau Basin back-arc spreading centre. Nature 346:646–648

Corry CE (1988) Laccoliths: Mechanics of emplacement and growth. Geol Soc Am Spec Pap 220

David J, Bailes AH, Machado N (1996) Evolution of the Snow Lake portion of the Paleoproterozoic Flin Flon and Kisseynew Belts, Trans-Hudson Orogen, Manitoba, Canada. Precambrian Res 80:107–124

Davis DW, Krogh TE, Hinzer J, Nakamura E (1985) Zircon dating of polycyclic volcanism at Sturgeon Lake and implications for base metal mineralization. Econ Geol 80:1942–1952

Detrick RS (1991) Ridge crest magma chambers: A review of results from marine seismic experiments at the East Pacific Rise. In: Peters TJ (ed) Ophiolite genesis and evolution of the oceanic lithosphere. Ministry of Petroleum and Minerals, Muscat, Sultanate of Oman, pp 7–20

Drummond MS, Defant MJ (1990) A model for trondhjemite-tonalite-dacite genesis and crustal growth via slab melting: Archean to modern comparisons. J Geophys Res 95:21503–21521

Fee J (1997) Geological, petrographic and geochemical study to determine the nature of alteration of a phase of the subvolcanic Sneath Lake pluton, Snow Lake, Manitoba. BSc Thesis, Laurentian University, Sudbury, Canada

Franklin JM, Lydon JW, Sangster DF (1981) Volcanic-associated massive sulfide deposits. Econ Geol 75th Anni vol, pp 485–627

Friske P (1974) The Beidelman Bay copper porphyry deposit. BSc Thesis, Lakehead University, Thunder Bay, Canada

Froose MP, Slack JF, Busby CJ, Schulz KJ, Scully MV (2002) Geological and structural setting of the Bald Mountain volcanogenic massive sulfide deposit, northern Maine. Soc Econ Geol Monogr 11 (in press)

Galley AG (1993) Semi-conformable alteration zones in volcanogenic massive sulfide districts. J Geochem Explor 48:175–200

Galley AG (1994) Geology of the Ansil Cu-Zn massive sulphide deposit, Rouyn-Noranda, Quebec, Canada. PhD Thesis, Carleton University, Canada

Galley AG (1996) Geochemical characteristics of subvolcanic intrusions associated with Precambrian massive sulfide districts.

In: Wyman DA (ed) Trace element geochemistry of volcanic rocks: applications for massive sulphide exploration. Geol Assoc Can Short Course 12:239–278

Galley AG, van Breemen O (2002) New U-Pb zircon dating constraints on the Flavrian-Powell subvolcanic intrusive complex and associated base metal mineralization. Geol Surv Can Curr Res Radiogenic Isot Stud (in press)

Galley AG, van Breemen O, Franklin JM (2000) The relationship between intrusion-hosted Cu-Mo mineralization and the VMS deposits of the Archean Sturgeon Lake mining camp, northwestern Ontario. Econ Geol 95:1543–1550

Gibson HL (1989) The mine sequence of the central Noranda volcanic complex: geology, alteration, massive sulphide deposits and volcanological reconstruction. PhD Thesis, Carleton University, Canada

Gibson HL, Watkinson DH (1990) Volcanogenic massive sulphide deposits of the Noranda cauldron and shield volcano, Quebec. In: Rive M, Gagnon Y, Lulin JM, Riverin G, Simard A (eds) The northwestern Quebec polymetallic belt. Can Inst Mineral Metall Spec vol 43:119–132

Gillis KM, Thompson G, Kelley DS (1993) A view of the lower crustal component of hydrothermal systems at the Mid-Atlantic Ridge. J Geophys Res 98:19597–19619

Goldie RJ (1976) The Flavrian and Powell Plutons, Noranda area, Quebec. PhD Thesis, Queen's University, Kingston, Canada

Goldie RJ (1978) Magma mixing in the Flavrian pluton, Noranda area, Quebec. Can J Earth Sci 15:132–144

Goldie RJ, Kotila B, Seward D (1979) The Don-Rouyn Mine: an Archean porphyry copper deposit near Noranda, Quebec. Econ Geol 74:1680–1684

Grant JA (1986) The isocon method – a simple solution to Gresens equations for metasomatic alteration. Econ Geol 81:1976–1982

Gregory RT, Taylor HP (1981) An oxygen isotope profile in a section of Cretaceous oceanic crust, Semail Ophiolite, Oman: Evidence for d18O buffering of the oceans by deep (>5 km) seawater-hydrothermal circulation at mid-ocean ridges. J Geophys Res 86:2737–2755

Hannington MD, Poulsen KH, Thompson JFH (1999) Volcanogenic gold in the massive sulfide environment. In: Barrie CT, Hannington MD (eds) Volcanic-associated massive sulfide deposits: processes and examples in modern and ancient settings. Rev Econ Geol 8:325–356

Hannington MD, Santaguida F, Kjarsgaard IM, Cathles LM (2002) Regional-scale hydrothermal alteration in the central Blake River Group, western Abitibi subprovince, Canada: implications for VMS prospectivity. Miner Deposita (in press) DOI 10.1007/s00126-002-0298-z

Haymon RM, Koski RA, Abrams MJ (1989) Hydrothermal discharge zones beneath massive sulfide deposits mapped in the Oman ophiolite. Geology 17:531–535

Hodder RW (1981) Evolution of an Archean felsic volcano-plutonic complex. Ontario Geol Surv Open File 5369

Hogan JP, Price JD, Gilbert MC (1998) Magma traps and driving pressure: consequences for plutonic shape and emplacement in an extensional regime: J Struct Geol 20:1155–1168

Hogan JP, Gilbert MC, Price JD (2000) Crystallization of fine- and coarse-grained A-type granite sheets of the Southern Oklahoma Aulacogen, U.S.A. Trans R Soc Edinb Earth Sci 91:139–150

Hudak GJ (1996) The physical volcanology and hydrothermal alteration associated with late caldera volcanic and volcaniclastic rocks and volcanogenic massive sulfide deposits in the Sturgeon Lake region of northwestern Ontario, Canada. PhD Thesis, University of Minnesota, Duluth

Huppert HE, Sparks RSJ (1988) The generation of granitic magmas by intrusion of basalt into continental crust. J Petrol 29:599–624

Huston DL (1993) The effect of alteration and metamorphism on wall rocks to the Balcooma and Dry River South volcanic-hosted massive sulfide deposits, Queensland, Australia. J Geochem Explor 48:277–307

Irvine TN, Baragar WRA (1971) A guide to the chemical classification of the common volcanic rocks. Can J Earth Sci 8:523–548

Jébrak M, Harnois L, Carriere A, Lafrance J (1997) The Don Rouyn Cu-Au porphyry system. In Couture JF, Robert F (eds) Atypical gold deposits in the Abitibi Belt, B5. GAC/MAC, Ottawa, pp 72–80

Johnson AM, Pollard DD (1973) Mechanics of growth of some laccolithic intrusions in the Henry Mountains, Utah. Part I. Tectonophysics 18:261–309

Kelley DS, Gillis KM (1993) Fluid evolution in submarine magma-hydrothermal systems at the Mid-Atlantic Ridge. J Geophys Res 98:19579–19596

Kennedy LP (1985) The geology and geochemistry of the Archean Flavrian Pluton, Noranda, Quebec. PhD Thesis, University of W. Ontario, London, Canada

Kesler SE, Jones LM, Walker RL (1975) Intrusive rocks associated with porphyry copper mineralization in island arc areas. Econ Geol 70:515–526

Lameyre J (1987) Granites and evolution of the crust. Rev Brasil Geosci 17:349–359

Lameyre J, Bowden P (1982) Plutonic rock types series: Discrimination of various granitiod series and related rocks. J Volcanol Geophys Res 14:169–186

Lang JR, Titley SR (1998) Isotopic and geochemical characteristics of Laramide systems in Arizona and implications for the genesis of porphyry copper deposits. Econ Geol 93:138-170

Langshur A (1991) The geology, geochemistry and structure of the Mooshla intrusion, Bousquet mining centre, Quebec. MSc Thesis, Ottawa University, Canada

Large RR, Doyle M, Raymond O, Cooke D, Jones A, Heasman L (1996) Evaluation of the role of Cambrian granites in the genesis of world class VHMS deposits in Tasmania. Ore Geol Rev 10:215–230

Leaman DE (1995) Mechanics of sill emplacement: comment based on the Tasmanian dolerites. Aust J Earth Sci 42:151–155

Le Maitre RW (1989) A classification of igneous rocks and glossary of terms. Blackwell, Oxford

Lesher CM, Goodwin AM, Campbell IH, Gorton MP (1985) Trace element geochemistry of ore-associated and barren felsic metavolcanic rocks in the Superior Province, Canada. Can J Earth Sci 23:222–237

Lister CRB (1972) On the thermal balance on a mid-ocean ridge. Geophys J R Astron Soc 26:515–535

Maier WD, Barnes S-J, Pellet T (1996) The economic significance of the Bell River Complex, Abitibi subprovince, Quebec. Can J Earth Sci 33:967–980

McLeod P, Stephen R, Sparks J (1998) The dynamics of xenolith assimilation. Contrib Mineral Petrol 132:21–33

Messenger PR, Golding SD (1996) Relationships between Devonian volcanic and plutonic units in the Mt. Morgan area, central Queensland. Austr J Earth Sci 43:97–101

Mével C, Cannat M (1991) Lithospheric stretching and hydrothermal processes in oceanic gabbros from slow-spreading ridges. In: Peters TJ (ed) Ophiolite genesis and evolution of the oceanic lithosphere. Ministry of Petroleum and Minerals, Muscat, Sultanate of Oman, pp 293–312

Moore PJ (1986) Geology of the high level plutonic rocks of the Troodos Ophiolite, Cyprus. BSc Thesis, Memorial University, Newfoundland

Mortensen JK (1993) U-Pb geochronology of the eastern Abitibi subprovince. Part 2. Noranda-Kirkland Lake area. Can J Earth Sci 30:29–41

Morton RL, Hudak GJ, Walke, JS, Franklin JM (1990) Physical volcanology and hydrothermal alteration of the Sturgeon Lake caldera complex. In: Franklin JM, Schneider BR, Koopman ER (eds) Mineral deposits in the Western Superior Province, Ontario. Geol Surv Can Open File 2164, pp 74–94

Nehlig P (1993) Interactions between magma chambers and hydrothermal systems: Oceanic and ophiolitic constraints. J Geophys Res 98:19621–19633

O'Connor JT (1965) A classification for quartz-rich igneous rocks based on feldspar ratios. USGS Prof Pap 1965:B79–B84

Pearce JA, Harris NBW, Tindle AG (1984) Trace element discrimination diagrams for the tectonic interpretation of granitic rocks. J Petrol 25:956–983

Peloquin AS, Potvin R, Paradis S, Lafleche MR, Verplaelst L, Gibson HL (1990) The Blake River Group, Rouyn-Noranda area, Quebec: A stratigraphic synthesis. In: Rive M (ed) The northwestern Quebec polymetallic belt. Can Inst Mining Metall Spec vol 43:107–118

Pilote P, Moorhead J, Mueller W (1998) Développement d'un arc volcanique, la région de Val d'Or, ceinture de l'Abitibi – Volcanologie, physique et évolution métallogénique. Geol Assoc Can Field Excur Guide A2

Poulsen KH, Franklin JM (1981) Copper and gold mineralization in an Archean trondhjemitic intrusion, Sturgeon Lake, Ontario. Geol Surv Can Curr Res A, pp 9–14

Poulsen KH, Hodgson CJ (1984) Mineralization associated with Archean gabbro-anorthosite intrusions, Rainy Lake area, northwestern Ontario. In: Guha J, Chown EH (eds) Chibougamau: stratigraphy and mineralization. Can Inst Mineral Metall 34:329–344

Richards MG (1999) Evolution of the Flavrian pluton and its association with the VHMS deposits and granitoid-hosted gold deposits of the Noranda Cauldron, Rouyn-Noranda, Quebec, Canada. PhD Thesis, Université de Montréal, Canada

Roman-Berdiel T, Gapais D, Brun JP (1995) Analogue models of laccolith formation. J Struct Geol 17:1337–1346

Russell JK, Edwards BR, Synder LD (1995) Volatile production possibilities during magmatic assimilation: heat and mass balance constraints. In: Thompson JFH (ed) Magmas, fluids, and ore deposits. Mineral Assoc Can 23:1–24

Sanborn-Barrie M, Skulski T, Parker J (2001) 300 m.y. of tectonic history recorded by the Red Lake greenstone belt, Ontario. Geol Surv Can Curr Res 2001(1C):15–22

Schutz W, Ebneth J, Klaus-Dieter M (1987) Trondhjemites, tonalites and diorites in the South Portuguese Zone and their relations to the vulcanites and mineral deposits of the Iberian Pyrite Belt. Geol Rundsch 76:201–212

Setterfield TN, Hodder RW, Gibson HL, Watkins JJ (1995) The McDougall-Despina fault set, Noranda, Quebec: Evidence for fault-controlled volcanism and hydrothermal fluid flow. Explor Mineral Geol 4:381–394

Sillitoe RH, Hannington MD, Thompson JFH (1996) High sulfidation deposits in the volcanogenic massive sulfide environment. Econ Geol 91:204–212

Singh SC, Collier JS, Harding AJ, Kent GM, Orcutt JA (1999) Seismic evidence for a hydrothermal layer above the solid roof of the axial magma chamber at the southern East Pacific Rise. Geology 27:219-222

Skirrow RG, Franklin JM (1994) Silicification and metal leaching in subconcordant alteration zones beneath the Chisel Lake massive sulfide deposit, Snow Lake, Manitoba. Econ Geol 89:31–50

Spooner ETC, Fyfe WS (1973) Sub-seafloor metamorphism, heat and mass transfer. Contrib Mineral Petrol 42:287–304

Spry A (1962) The origin of columnar jointing, particularly in basalt flows. J Geol Soc Austr 8:191–216

Stakes DS, Taylor HP (1992) The northern Semail ophiolite: an oxygen isotope, microprobe, and field study. J Geophys Res 97:7043–7080

Stein G, Thiéblemont D, Leistel J-M (1996) Relations volcanisme/plutonisme dans la Ceinture pyriteuse ibérique, secteur de Campfrío, Espagne. C R Acad Sci Paris 322:1021–1028

Stern RA, Syme EC, Bailes AH, Lucas SB (1995) Paleoproterozoic (1.90–1.86 Ga) arc volcanism in the Flin Flon Belt, Trans-Hudson Orogen, Canada. Contrib Mineral Petrol 119:117–141

Stinton JM, Detrick RS (1992) Mid-ocean ridge magma chambers. J Geophys Res 97:197–216

Sun SS, McDonough WF (1989) Chemical and isotopic systematics of oceanic basalts: implications for mantle composition and

process. In: Saunders AD, Norry MJ (eds) Magmatism and ocean basins. Geol Soc Lond, pp 313–345

Taylor BE, Holk GJ (1998) Stable isotope applications in the exploration for volcanic-associated massive sulfide deposits: a preliminary summary. In: 3rd Annu Rep CAMIRO, Toronto, Proj 94E07, 3, pp 40–47

Taylor BE, South BC (1985) Regional stable isotope systematics of hydrothermal alteration and massive sulfide deposition in the West Shasta District, California. Econ Geol 80:2149–2163

Thiéblemont D, Pascual E, Stein G (1998) Magmatism in the Iberian Pyrite Belt: petrological constraints on a metallogenic model. Miner Deposita 33:98–110

Trowell NF (1974) Geology of the Bell Lake-Sturgeon Lake area, districts of Thunder Bay and Kenora. Ontario Geol Surv Rep 114, p 67

Trudel P (1978) Géologie de la région de Cléricy, Québec. Ministère Rich Nat Québec Rapp DP-598

Von Damm KL (1995) Controls on the chemistry and temporal variability of seafloor hydrothermal fluids. In: Humphris SE, Zierenberg RA, Mullineaux LS, Thomson RE (eds) Seafloor hydrothermal systems: physical, chemical, biological, and geological interactions. Am Geophys Union Monogr 91:222–272

Walford PC, Franklin JM (1982) The Anderson Lake Mine, Snow Lake, Manitoba. In: Hutchinson RW, Franklin JM (eds) Precambrian sulphide deposits. Geol Assoc Can Spec Pap 25: 481–523

Weihed P (1991) Age of porphyry-type deposits in the Skellefte District, northern Sweden. J Geol Fören Stockholm Förhand 113:289–294

Weihed P (1992) Geology and genesis of the Early Proterozoic Tallberg porphyry-type deposit, Skellefte District, northern Sweden. Geol Inst A72:147

Whalen JB (1985) Geochemistry of an island-arc plutonic suite: the Uasilau-Yau Yau intrusive complex, New Britain, P.N.G. J Petrol 26:603–632

Winchester JA, Floyd PA (1975) Geochemical magma type discrimination: application to altered and metamorphosed basic igneous rocks. Earth Planet Sci Lett 28:459–469

Witt WK (1999) The Archean Ravensthorpe Terrane, Western Australia: synvolcanic Cu-Au mineralization in a deformed island arc complex. Precambrian Res 96:143–181

Yang K, Scott SD (1996) Possible contribution of a metal-rich magmatic fluid to a seafloor hydrothermal system. Nature 383:420–423

Zaleski E, Peterson V (1995) Depositional setting and deformation of massive sulfide deposits, iron formation, and associated alteration in the Manitouwadge greenstone belt, Superior Province, Ontario. Econ Geol 90:2244–2261